Cell Reports

Report

WDR47 protects neuronal microtubule minus ends from katanin-mediated severing

Graphical abstract

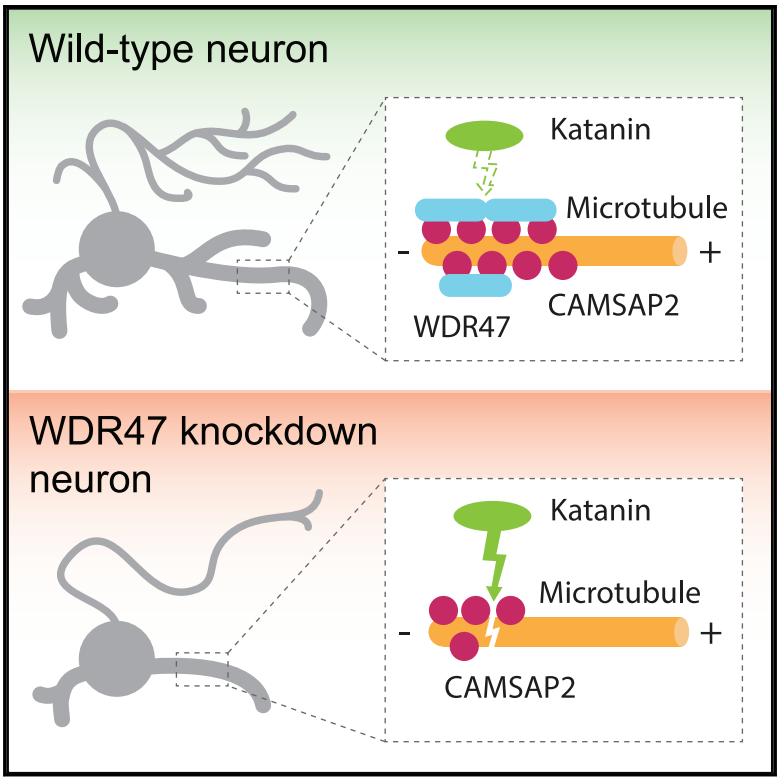

Authors

Robin R. Buijs, Jessica J.A. Hummel, Mithila Burute, ..., Anna Akhmanova, Lukas C. Kapitein, Casper C. Hoogenraad

Correspondence

c.hoogenraad@uu.nl

In brief

Noncentrosomal microtubules in neurons are stabilized by CAMSAP minus-end binding proteins, but how CAMSAPs are regulated in neurons remains unclear. Buijs et al. identify WDR47 as an essential player involved in regulation of CAMSAP-positive microtubule minus ends in neurons and propose a model where WDR47 protects CAMSAP2 against katanin-mediated severing.

Highlights

- WDR47 is required for axonal and dendritic development
- WDR47 colocalizes with CAMSAP family proteins in axon and dendrites
- WDR47 is critical for maintenance of CAMSAP2-positive microtubule stretches
- WDR47 prevents katanin-mediated severing of microtubule minus ends

Buijs et al., 2021, Cell Reports *36*, 109371
July 13, 2021
https://doi.org/10.1016/j.celrep.2021.109371

CellPress

Cell Reports

CellPress
OPEN ACCESS

Report

WDR47 protects neuronal microtubule minus ends from katanin-mediated severing

Robin R. Buijs,[1] Jessica J.A. Hummel,[1] Mithila Burute,[1] Xingxiu Pan,[1] Yujie Cao,[1] Riccardo Stucchi,[1,2] Maarten Altelaar,[2] Anna Akhmanova,[1] Lukas C. Kapitein,[1] and Casper C. Hoogenraad[1,3,4,*]

[1]Cell Biology, Neurobiology and Biophysics, Department of Biology, Faculty of Science, Utrecht University, 3584 Utrecht, the Netherlands
[2]Biomolecular Mass Spectrometry and Proteomics, Bijvoet Center for Biomolecular Research and Utrecht Institute for Pharmaceutical Sciences, Utrecht University, 3584 Utrecht, the Netherlands
[3]Department of Neuroscience, Genentech, Inc., South San Francisco, CA 94080, USA
[4]Lead contact
*Correspondence: c.hoogenraad@uu.nl
https://doi.org/10.1016/j.celrep.2021.109371

SUMMARY

Axons and dendrites are long extensions of neurons that contain arrays of noncentrosomal microtubules. Calmodulin-regulated spectrin-associated proteins (CAMSAPs) bind to and stabilize free microtubule minus ends and are critical for proper neuronal development and function. Previous studies have shown that the microtubule-severing ATPase katanin interacts with CAMSAPs and limits the length of CAMSAP-decorated microtubule stretches. However, how CAMSAP and microtubule minus end dynamics are regulated in neurons is poorly understood. Here, we show that the neuron-enriched protein WDR47 interacts with CAMSAPs and is critical for axon and dendrite development. We find that WDR47 accumulates at CAMSAP2-decorated microtubules, is essential for maintaining CAMSAP2 stretches, and protects minus ends from katanin-mediated severing. We propose a model where WDR47 protects CAMSAP2 at microtubule minus ends from katanin activity to ensure proper stabilization of the neuronal microtubule network.

INTRODUCTION

In neurons, several processes, such as migration, polarization, plasticity, and development, rely on proper organization of the microtubule (MT) cytoskeleton. MTs provide structural support to ensure specialized cell morphology, act as scaffolds for organelle positioning, and facilitate intracellular transport, for which molecular motors recognize and use the intrinsic polarity of MTs to transport cargo in a directional manner (Conde and Cáceres, 2009; Kapitein and Hoogenraad, 2015). This intrinsic polarity results in MTs having two structurally and functionally different ends, the plus and minus end, that each display distinct behavior in living cells. Many studies in the last decade have focused on the highly dynamic plus ends, which show periods of rapid growth and shortening and are regulated by MT plus end tracking proteins (+TIPs) (Akhmanova and Hoogenraad, 2005; Akhmanova and Steinmetz, 2008). In contrast, the relatively stable MT minus ends remain poorly studied even though their organization is of fundamental importance for the architecture of cellular MT arrays (Dammermann et al., 2003; Akhmanova and Hoogenraad, 2015). At first, the only protein complex known to specifically associate with MT minus ends was the γ-tubulin ring complex (γ-TuRC), which facilitates MT nucleation (Kollman et al., 2011; Teixidó-Travesa et al., 2012). In recent years, significant progress has been made in understanding the mechanisms that regulate the behavior and organization of MT minus ends (Akhmanova and Hoogenraad, 2015; Akhmanova and Steinmetz, 2015). Our understanding of MT minus end dynamics advanced substantially with discovery of the calmodulin-regulated spectrin-associated protein (CAMSAP) family of proteins, which specifically associate with MT minus ends. This function was initially characterized for Nezha/CAMSAP3, which binds MT minus ends and tethers them to adherens junctions (Meng et al., 2008). Three mammalian members of this family were identified in total: CAMSAP1, CAMSAP2, and CAMSAP3/Nezha (Baines et al., 2009). In addition, the invertebrate homolog Patronin is also able to recognize MT minus ends and protect them from depolymerization (Goodwin and Vale, 2010). *In vitro* reconstitutions elucidated that CAMSAP1 dynamically tracks growing MT minus ends, whereas CAMSAP2 and CAMSAP3 are deposited on the MT lattice at the elongating minus end (Jiang et al., 2014). As a result, CAMSAP2 and CAMSAP3 stabilize MT minus ends and thereby contribute to maintenance of the MT cytoskeleton (Tanaka et al., 2012). Because of this, CAMSAP2 and CAMSAP3 are required for neuronal polarity and development (Yau et al., 2014; Pongrakhananon et al., 2018). CAMSAP1 has also been shown to play a role in neuronal polarization and migration by regulating the MT cytoskeleton as a substrate of the polarity regulator MARK2 kinase (Zhou et al., 2020). Interestingly, previous studies have shown that the MT-severing ATPase katanin interacts with CAMSAP2 and CAMSAP3 and limits the length of CAMSAP-decorated MT stretches (Jiang et al., 2014, 2018). However, little is known about the role of katanin in regulation of CAMSAPs at MT minus ends in neurons.

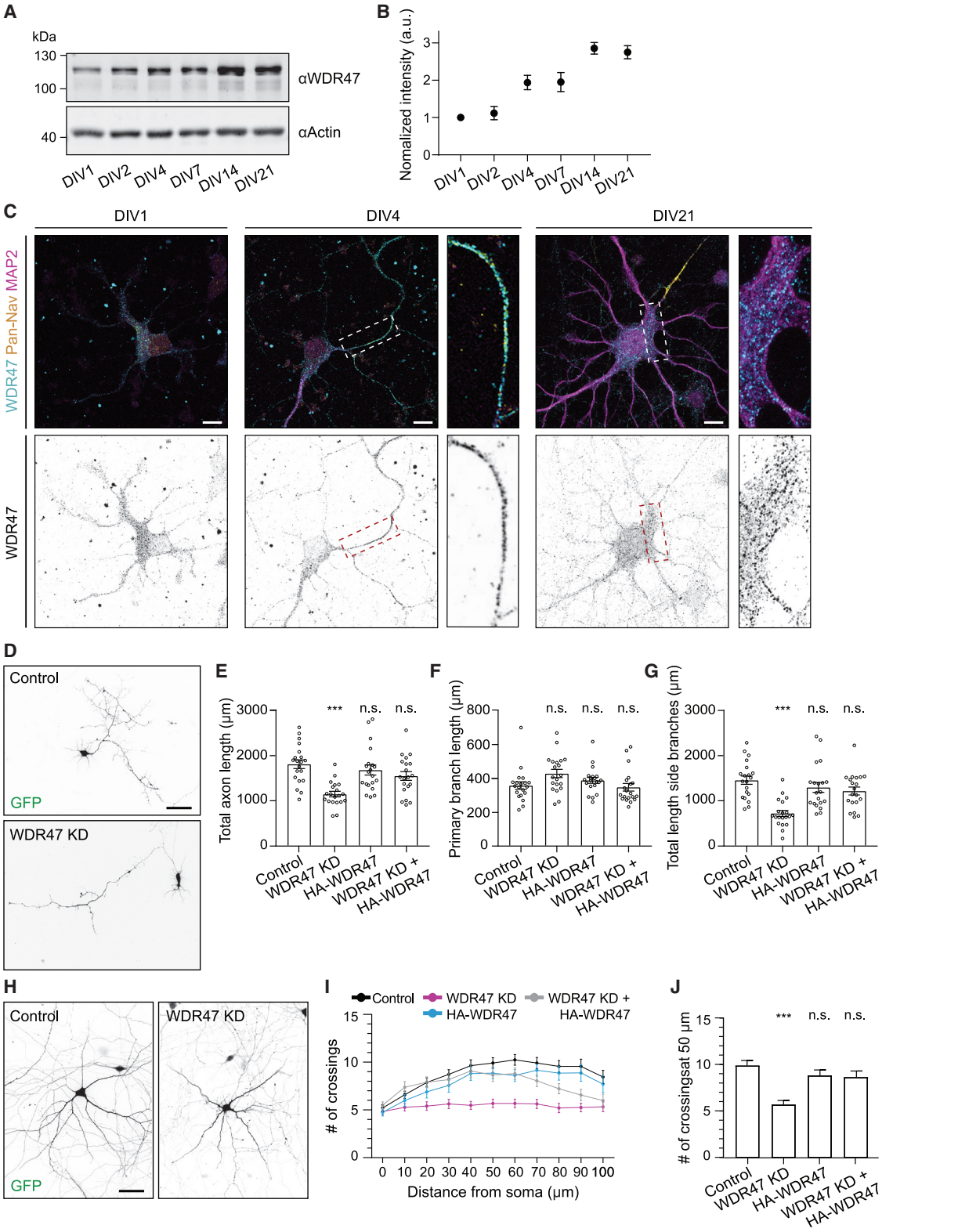

(legend on next page)

WD repeat containing protein 47 (WDR47, also known as Nemitin) belongs to the WD40 repeat family and is highly enriched in the brain and expressed specifically in neurons (Wang et al., 2012). The CNS function of WDR47 is essential for mouse survival (Kannan et al., 2017; Chen et al., 2020). WDR47-deficient brains lack major axonal tracts and display deficient neuronal radial migration and multipolar-bipolar transition (Kannan et al., 2017). Recently, WDR47 has been shown to cooperate with CAMSAP3 in regulating neuronal polarization (Chen et al., 2020). How WDR47 regulates MT minus-end dynamics and affect neuronal development remains unclear. In this study, we show that WDR47 colocalizes with CAMSAP-decorated MT minus ends in axonal and dendritic compartments and is essential for both early and later stages of neuronal development. We find that WDR47 is essential for the maintenance of CAMSAP2 stretches in neurons and protects them against katanin-mediated severing. We propose a model where WDR47 protects CAMSAP2 at MT minus ends from katanin to ensure proper stabilization of the MT network during neuronal development.

RESULTS

WDR47 is important for neuronal development

We first determined WDR47 protein expression levels in dissociated rat cortical neurons in culture. WDR47 was detected during early neuronal development in lysates harvested at days *in vitro* (DIV) 1–2, increased ~2-fold at DIV4 and DIV7, a period characterized by axonal growth, and reached an ~3-fold increase around DIV14–DIV21, when dendrites develop (Figures 1A and 1B). Visualizing the cellular localization of endogenous WDR47 displayed a punctate pattern throughout the cytoplasm in young hippocampal neurons that, upon polarization and axon outgrowth, remained punctated but became enriched in the proximal axon. In mature neurons, WDR47 becomes increasingly visible as puncta within the somatodendritic compartment that sometimes show a stretch-like pattern (Figure 1C). Exogenous WDR47 shows a more substantial diffuse pool with enrichment in the proximal axon and also localizes as puncta and short stretches throughout the somata and dendrites in live neurons (Figure S1A).

To examine the function of WDR47 in neurons, first three independent short hairpin RNAs (shRNAs) targeting rat WDR47 were designed. Western blot validation showed efficient reduction of WDR47 protein levels with shRNA#1 and shRNA#3 and the combination of both (Figures S1B and S1C). Immunostaining confirmed that WDR47 intensity was reduced strongly in hippocampal neurons upon depletion of WDR47 (Figure S1D). To determine the role of WDR47 in early neuronal development, we depleted WDR47 immediately after neuronal isolation. Knockdown of WDR47 resulted in a reduced number of polarized neurons at DIV2 and DIV4 (Figures S1E and S1F). Upon close examination of DIV4 neuronal morphology, we found that WDR47 depletion impaired axonal growth because total axon length was decreased significantly compared with controls (Figures 1D and 1E). Further analysis revealed that this reduction is mainly due to loss of axonal branches, whereas the primary axon is less affected and becomes slightly longer (Figures 1F and 1G). Co-expression of human WDR47 restored the WDR47 levels as validated by western blot (Figure S1G) and rescued the axonal phenotype (Figures 1D–1G). Both validated WDR47 shRNAs affected axonal morphology in a similar manner (Figures S1H–S1J). We also investigated the effect of WDR47 depletion on dendritic development at DIV11 using Sholl analysis and observed a reduction in total dendritic branching and complexity compared with controls. Co-expression of WDR47 alleviated this affect (Figures 1H–1J). Collectively, these data show that WDR47 is required during early and late developmental stages of cultured hippocampal neurons.

WDR47 interacts with different CAMSAPs in specific neuronal compartments

To gain more mechanistic insights into the role of WDR47, we searched for its putative binding partners in rat brain extract using affinity purification-mass spectrometry (AP-MS). Among the list of putative interaction proteins we identified all three members of the CAMSAP family (Figure 2A; Table S2), consistent with equivalent findings using mouse brain lysates recently reported (Chen et al., 2020). Our proteomics results were validated by pull-down experiments showing that HA-CAMSAP1, HA-CAMSAP2, and HA-CAMSAP3 bind to GFP-WDR47 but not to the control GFP (Figure 2B).

To further investigate this interaction of CAMSAP family proteins with WDR47, we designed truncated constructs of the

Figure 1. WDR47 is important for neuronal development

(A) Western blot analysis of lysates from DIV1, DIV2, DIV4, DIV7, DIV14, and DIV21 cortical neurons with the indicated antibodies.

(B) Quantification of WDR47 levels related to (A). Data are normalized to actin (loading control) and WDR47 levels at DIV1 (N = 2, n = 4).

(C) Representative images of DIV1, DIV4, and DIV21 hippocampal neurons stained for WDR47 (cyan), Pan-Nav (yellow) and MAP2 (magenta). Magnifications are indicated by dashed boxes.

(D) Wide-field images of DIV4 hippocampal neurons electroporated at DIV0 with GFP and pSuper control or WDR47 shRNA#1+3 (WDR47 knockdown [KD]). Related to Figures S1H–S1J.

(E) Quantification of the total axon length of DIV4 hippocampal neurons co-transfected for 96 h with GFP, pSuper control, or WDR47 shRNA#3 (WDR47 KD) and HA or HA-WDR47 (N = 2, n = 20).

(F) Quantification of the longest axon branch of DIV4 hippocampal neurons co-transfected for 96 h with GFP, pSuper control, or WDR47 shRNA#3 (WDR47 KD) and HA or HA-WDR47 (N = 2, n = 20).

(G) Quantification of the total length of all side branches of DIV4 hippocampal neurons co-transfected for 96 h with GFP, pSuper control, or WDR47 shRNA#3 (WDR47 KD) and HA or HA-WDR47 (N = 2, n = 20).

(H) Wide-field images of DIV11 hippocampal neurons co-transfected for 96 h with GFP, pSuper control, or WDR47 shRNA#3 (WDR47 KD). See also (I) and (J).

(I) Sholl analysis of DIV11 hippocampal neurons co-transfected for 96 h with GFP, pSuper control, or WDR47 shRNA#3 (WDR47 KD) and HA or HA-WDR47 (N = 2, n = 20).

(J) Average number of crossings at 50-μm distance from the soma; see also (I) (N = 2, n = 20).

Graphs represent mean ± SEM. ***$p < 0.001$. See also Figure S1 and Table S1. Scale bars, 10 μm in (C) and 50 μm in (D) and (H).

A

Rat brain

Description	Count	Bio-GFP	Bio-GFP-WDR47
CAMSAP1	#Peptides		35
	#PSM		60
CAMSAP2	#Peptides		48
	#PSM		135
CAMSAP3	#Peptides		47
	#PSM		155

B

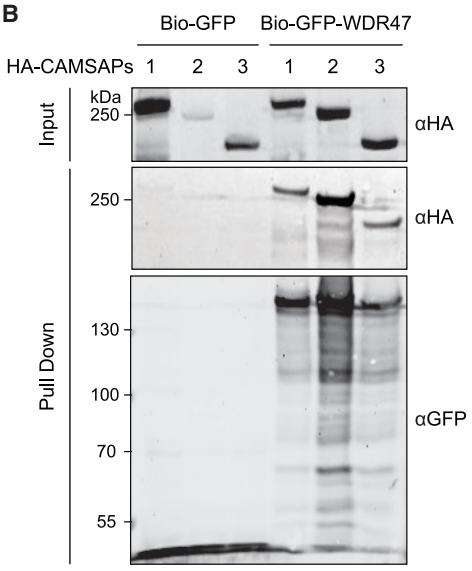

C

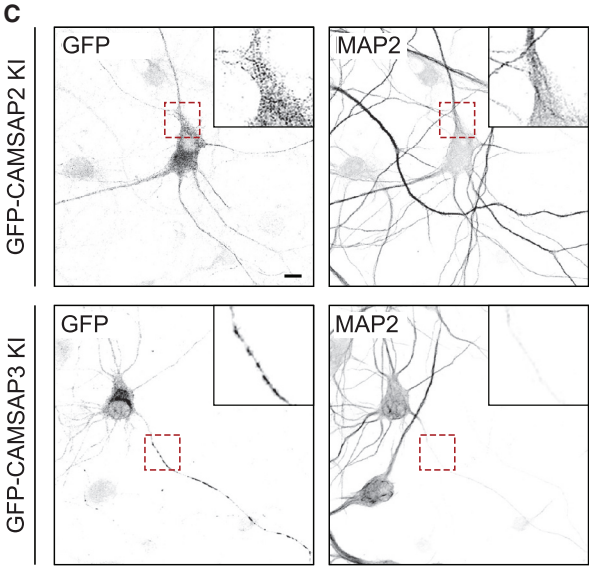

D

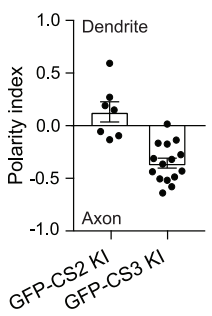

E

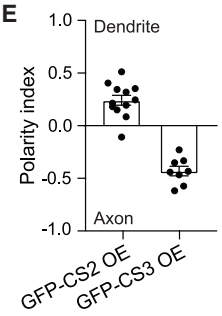

F

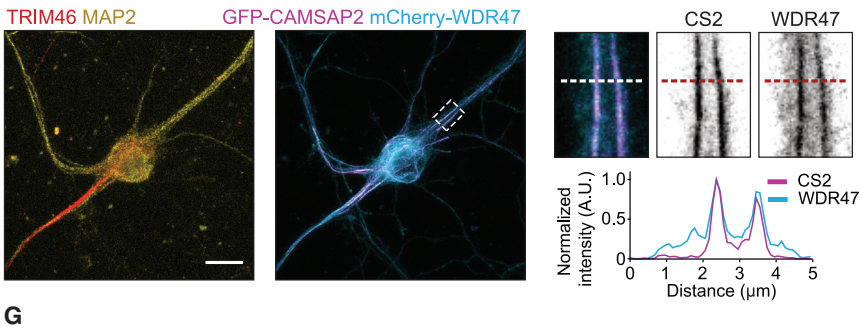

G

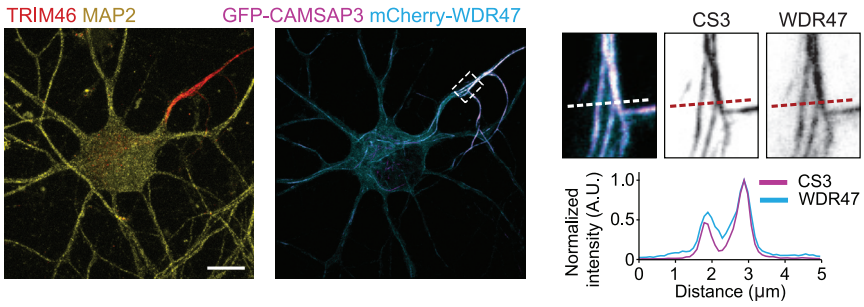

(legend on next page)

N- and C-terminal regions of WDR47 (Figure S2A). Using these WDR47 truncations as prey, pull-down experiments showed that all three CAMSAPs interact with WDR47_N and WDR47_C (Figures S2B–S2D). Interestingly, CAMSAP2 showed strong binding to the C-terminal region of WDR47 specifically, whereas CAMSAP1 and CAMSAP3 interacted in equal amounts with both WDR47 truncations. Using CAMSAP2 and CAMSAP3 as prey, we again detected increased binding of WDR47_C specifically to CAMSAP2 (Figures S2E and S2F).

Because CAMSAP2 and CAMSAP3 strongly contribute to maintenance of the MT cytoskeleton with their major role in generation of stable MT minus ends that facilitate MT regrowth, we set out to determine their relationship with WDR47 by looking at their subcellular localization in hippocampal neurons. We used the homology-independent targeted integration (HITI) CRISPR knockin system to integrate a GFP tag into the genes of CAMSAP2 and CAMSAP3 in hippocampal neurons, which revealed that endogenous CAMSAP3 shows preferred localization in the axon. Endogenous CAMSAP2, on the other hand, was mainly visible in the somatodendritic compartment but not excluded from the axon (Figures 2C and 2D). Overexpression of GFP-CAMSAP2 and GFP-CAMSAP3 gave a very similar subcellular distribution, confirming proper localization of the exogenous GFP constructs (Figure 2E). When combining exogenous CAMSAP2 and CAMSAP3 with mCherry-WDR47, we observed marked colocalization of WDR47 with CAMSAP2 and CAMSAP3 in cell bodies and dendrites and axons, respectively (Figures 2F and 2G). Colocalization was also observed between clusters of GFP-tagged WDR47 and endogenous CAMSAP2 puncta and vice versa (Figures S2G and S2H). Together, these results suggest that WDR47 interacts with CAMSAP family members and colocalizes with CAMSAP3 predominantly in the axon and with CAMSAP2 in the somatodendritic region of mature neurons.

WDR47 localizes to MT minus ends along with CAMSAP2

To gain insight into WDR47 and CAMSAP2 localization, we used total internal reflection fluorescence (TIRF) microscopy to image COS-7 cells expressing low levels of GFP-tagged CAMSAP2 and mCherry-tagged WDR47, in which we colored the MT cytoskeleton using low-dose silicon rhodamine (SiR)-tubulin. CAMSAP2 localized as puncta and short stretches throughout the cytoplasm at MT ends. WDR47 was more diffuse but also clearly localized with CAMSAP2 at MT minus ends (Figure 3A). While all WDR47 puncta colocalized with CAMSAP2, some CAMSAP2 puncta did not coincide with WDR47 (Figure 3B). Using automated particle detection and colocalization analysis, we found that CAMSAP2 puncta that colocalize with WDR47 have higher CAMSAP2 intensity (Figure 3C), area (Figure 3D), and especially higher CAMSAP2 density (Figure 3E) compared with CAMSAP2 puncta that do not colocalize with WDR47. To determine the dynamic relationship between WDR47 and CAMSAP2 localization at the MT minus ends, we performed MT severing using laser ablation to generate new minus ends of MTs. Interestingly, WDR47 did not accumulate at the new MT minus end that was captured and stabilized by CAMSAP2 after MT severing (Figures S3A–S3C; Video S1). However, live monitoring of CAMSAP2 puncta revealed that WDR47 localizes and enriches to dense CAMSAP2 puncta that are growing into a stretch-like structure (Figure S3D; Video S2). These results suggest that WDR47 is recruited to CAMSAP2 at MT minus ends when a CAMSAP2 punctum is growing into a stretch.

To further investigate the functional connection between WDR47 and CAMSAP2, we designed new truncated constructs based on protein domains and examined their interaction using pull-down assays (Figure 3F and 3G). Using full-length WDR47 as bait, we detected binding of full-length CAMSAP2 and the CAMSAP2_Middle truncation (Figures 3F and S3E). Conversely, full-length CAMSAP2 was able to pull down full-length WDR47 as well as the WDR47_Middle and WDR47_WD40 truncations but not the WDR47_LisH-CTLH truncation. Using CAMSAP2_Middle as bait, we found that this domain interacts specifically with the WDR47_WD40 truncation (Figures 3G and S3F). These results suggest that WDR47 contains two separate binding sites for CAMSAP2: the WD40 domain and WDR47_Middle region.

WDR47 knockdown affects endogenous CAMSAP2 stretches

Previous data indicated that CAMSAP2 associates with MT minus ends by itself (Jiang et al., 2014), and we showed that WDR47 localizes to CAMSAP2-positive MT minus ends (Figure 3). To test whether CAMSAP2 stretches depend on WDR47, we depleted WDR47 in DIV8 neurons. Upon WDR47 knockdown, endogenous CAMSAP2 shows a diffuse cytoplasmic signal without the typical punctuated stretches (Figure 4A). Quantification revealed a strong reduction of CAMSAP2 stretches in the soma (Figures 4B, 4C, and S4A). To control for variation in staining between samples, we included non-transfected neurons of each coverslip in our analysis for normalization. Interestingly, co-expression of HA-WDR47 could rescue the observed phenotype, whereas transfection with HA-WDR47 alone did not affect the analyzed parameters (Figures

Figure 2. WDR47 interacts with CAMSAP3 in the axon and with CAMSAP2 in the somatodendritic compartment

(A) CAMSAP binding partners of Bio-GFP-WDR47 in rat brain lysates, identified by AP-MS.

(B) Western blot analysis of the streptavidin pull-down assay using extracts of HEK293T cells transfected with BirA and HA-CAMSAP1, HA-CAMSAP2 or HA-CAMSAP3 (bait) and Bio-GFP-WDR47 or Bio-GFP (prey) as a negative control with the indicated antibodies.

(C) Representative images of DIV11 hippocampal neurons transfected with the HITI CRISPR knockin (KI) constructs GFP-CAMSAP2KI and GFP-CAMSAP3 KI stained for MAP2 and GFP (to enhance the signal in transfected cells). Magnifications are indicated by dashed boxes.

(D) Polarity index of the CRISPR KI constructs GFP-CAMSAP2 KI and GFP-CAMSAP3 KI; see also (C) (N = 2, n = 7–15).

(E) Polarity index of the exogenous constructs GFP-CAMSAP2 overexpression (OE) and GFP-CAMSAP3 OE in DIV11 hippocampal neurons (N = 2, n = 8–12).

(F and G) Representative images of DIV11 hippocampal neurons transfected with GFP-CAMSAP2 (F) or GFP-CAMSAP3 (G) and mCherry-WDR47. Magnifications are indicated by dashed boxes and show examples of a dendrite (F) or axon (G) based on the presence/absence of MAP2 (yellow) and TRIM46 (red) staining. Intensity profiles show the normalized intensity of both transfected constructs along the dashed line indicated in the magnifications.

Graphs represent mean ± SEM. See also Figure S2 and Table S1. Scale bars, 10 μm.

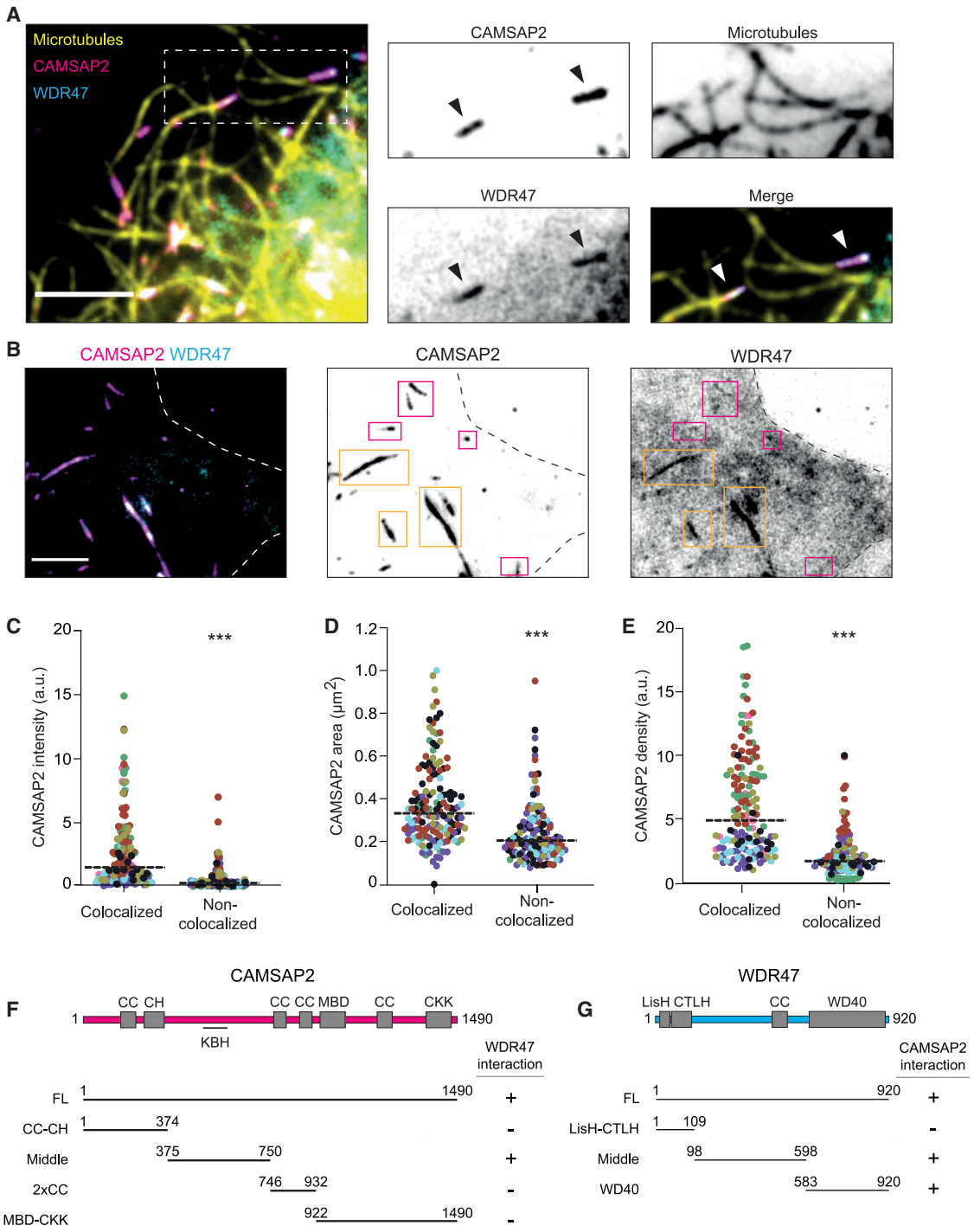

Figure 3. WDR47 localizes to MT minus ends along with CAMSAP2

(A) TIRF image of a COS-7 cell with MTs stained using SiR-tubulin (yellow), transfected with 3GFP-CAMSAP2 (magenta) and mCherry-WDR47 (cyan). Magnification is indicated by a dashed box, and arrows indicate MT minus ends.

(B) TIRF image of COS-7 cell transfected with 3GFP-CAMSAP2 (magenta), mCherry-WDR47 (cyan), and SiR-tubulin (data not shown) for stretch detection and colocalization analysis. Yellow boxes indicate CAMSAP2 puncta that colocalized with WDR47, and magenta boxes indicate puncta that do not colocalize.

(C–E) Quantification of the intensity (C), area (D), and density (intensity/area; E) of automatically detected CAMSAP2 puncta. Puncta are categorized into two groups based on their colocalization with WDR47. Each color indicates puncta from the same cell. Dotted lines indicate the group mean.

(legend continued on next page)

4A–4C and S4A). These findings suggest that WDR47 is critical for the maintenance of CAMSAP2 stretches in neurons.

WDR47 protects CAMSAP2 stretches from katanin

Based on our data, it is tempting to speculate that WDR47 is protecting CAMSAP2-decorated MT minus ends from additional regulating factors. A candidate protein known to affect the length of CAMSAP2 stretches is the MT-severing enzyme katanin. Katanin consists of a catalytic subunit, p60, which belongs to the ATPases Associated with diverse cellular Activities (AAA+) family, and a regulatory p80 subunit (McNally and Vale, 1993; Hartman et al., 1998; Roll-Mecak and McNally, 2010). Katanin interacts with a short helical motif between amino acids (aa) 477–574 of CAMSAP2, and this interaction is required for katanin to limit the length of CAMSAP2-decorated MT stretches (Jiang et al., 2014). Interestingly, this katanin-binding helix is localized in the region of the truncation CAMSAP2_Middle (Figure 2F), which, according to our biochemical data, is involved in the interaction with WDR47.

To determine whether katanin affects CAMSAP2 stretch length in neurons, we transfected DIV8 hippocampal neurons for 2 days with the p60 and p80 subunits. Katanin expression had a strong effect on endogenous CAMSAP2, which lost its distinct stretches, with the majority of the neurons showing only small CAMSAP2 puncta (1–2 μm) (Figures 4D, 4E, and S4B). Co-expression of katanin and HA-WDR47 resulted in a mixed population of neurons, with 17% showing only CAMSAP2 puncta, 31% showing the typical long CAMSAP2 stretches (>10 μm) and 52% showing an intermediate pattern of endogenous CAMSAP2 with relatively short CAMSAP2 stretches (3–10 μm). In these cells, WDR47 exhibited a diffuse pool but also accumulated at the endogenous CAMSAP2 stretches (Figures 4D, 4E, and S4B). Further experiments revealed that expression of the katanin p60 subunit alone, but not katanin p80, was sufficient to alter the localization pattern of endogenous CAMSAP2 (Figures S4B–S4D). Co-expression of WDR47 and katanin p60 partially rescued the change in localization of endogenous CAMSAP2 observed in p60-expressing neurons (Figures S4B–S4D). Furthermore, Sholl analysis revealed that katanin expression severely affects the complexity of the dendritic tree and that co-expressing HA-WDR47 partly rescues this phenotype (Figures 4F, 4G, and S4E). These results suggest that WDR47 can prevent katanin-mediated severing of CAMSAP2 stretches.

DISCUSSION

CAMSAP minus-end binding proteins play an essential role in the stabilization of noncentrosomal MTs in neurons (Akhmanova and Hoogenraad, 2015). Here we identify WDR47 as an important player involved in regulation of CAMSAP-positive MT minus ends in neurons. We show that the interplay between WDR47 and katanin is important for CAMSAP2-stabilized noncentrosomal MT minus ends. Similar to MT plus-end dynamics, our data demonstrate that neuronal MT minus ends are subject to an intricate balance of multiple competing factors and regulatory mechanisms.

WDR47 interacts with CAMSAP family proteins and is critical for neuronal development

WDR47 is a neuron-enriched protein that is critical for *in vivo* brain development (Kannan et al., 2017). Here we find that WDR47 plays an important role during early neuronal polarization, in agreement with recent findings (Chen et al., 2020), and later stages of neuronal development. We found that WDR47 interacts strongly with CAMSAP family proteins. In contrast to a previous study (Chen et al., 2020), our data suggest that the N- and C-terminal regions of WDR47 are involved in CAMSAP interaction. In addition, we observed that WDR47 colocalizes with CAMSAP2 and CAMSAP3 in neurons. CAMSAP3 is found predominantly in the axon, consistent with its role in axon development (Pongrakhananon et al., 2018; Chen et al., 2020). In maturing neurons, CAMSAP2 is localized predominantly in the somatodendritic compartment, correlating with its role in dendrite development and the stabilization of the dendritic MT cytoskeleton (Yau et al., 2014). Interestingly, in younger neurons (stage 3), CAMSAP2 has been found to be distributed throughout all neurites (Pongrakhananon et al., 2018), suggesting that the subcellular localization of CAMSAP2 is tightly regulated throughout neuronal development. CAMSAP1 has been shown to play a role in neuronal polarization and migration by regulating the MT cytoskeleton as a substrate of the polarity regulator MARK2 kinase (Zhou et al., 2020). It is evident that the different CAMSAPs have diverged and contribute to neuronal development in specific manners. Further research is needed to elucidate the details of their specialized functions.

It is generally believed that the presence of CAMSAP2 is sufficient to ensure MT minus end stabilization. *In vitro* reconstitutions showed that CAMSAP2 associates rapidly with free MT minus ends and is deposited on the MT lattice at the elongating MT minus end. These stable CAMSAP2 stretches prevent MT depolymerization and serve as seeds for MT regrowth (Hendershott and Vale, 2014; Jiang et al., 2014). Interestingly, we discovered that, in neurons, WDR47 is essential for the maintenance of CAMSAP2 stretches because endogenous CAMSAP2 stretches disappear in neurons depleted from WDR47. In addition, our live imaging experiments suggest that WDR47 has a positive effect on CAMSAP2 stretches because CAMSAP2 intensity increases when WDR47 is present. We confirm that CAMSAP2 associates with MT minus ends, which is followed by recruitment of WDR47, and the proteins accumulate together over time. When WDR47 is recruited at the MT minus end, it is possible that WDR47, in concert with other factors, may prevent CAMSAP2 loss and mediate recruitment of

(F) Schematic of the domain structure of CAMSAP2 and the constructs/truncations used for the pull-downs shown in Figure S3. Indicated domains: CC, coiled coil; CH, calponin-homology domain; CKK, CKK domain; MBD, MT-binding domain. KBH indicates the location of the katanin-binding helix.
(G) Schematic depiction of the domain structure of WDR47 and the constructs/truncations used for the pull-downs shown in Figure S3. Indicated domains: CC, coiled coil; CTLH, C-terminal to LisH domain; LisH, lissencephaly-1 homology domain; WD40, WD40 repeat domain.
***$p < 0.001$. See also Figure S3 and Table S1. Scale bars, 5 μm.

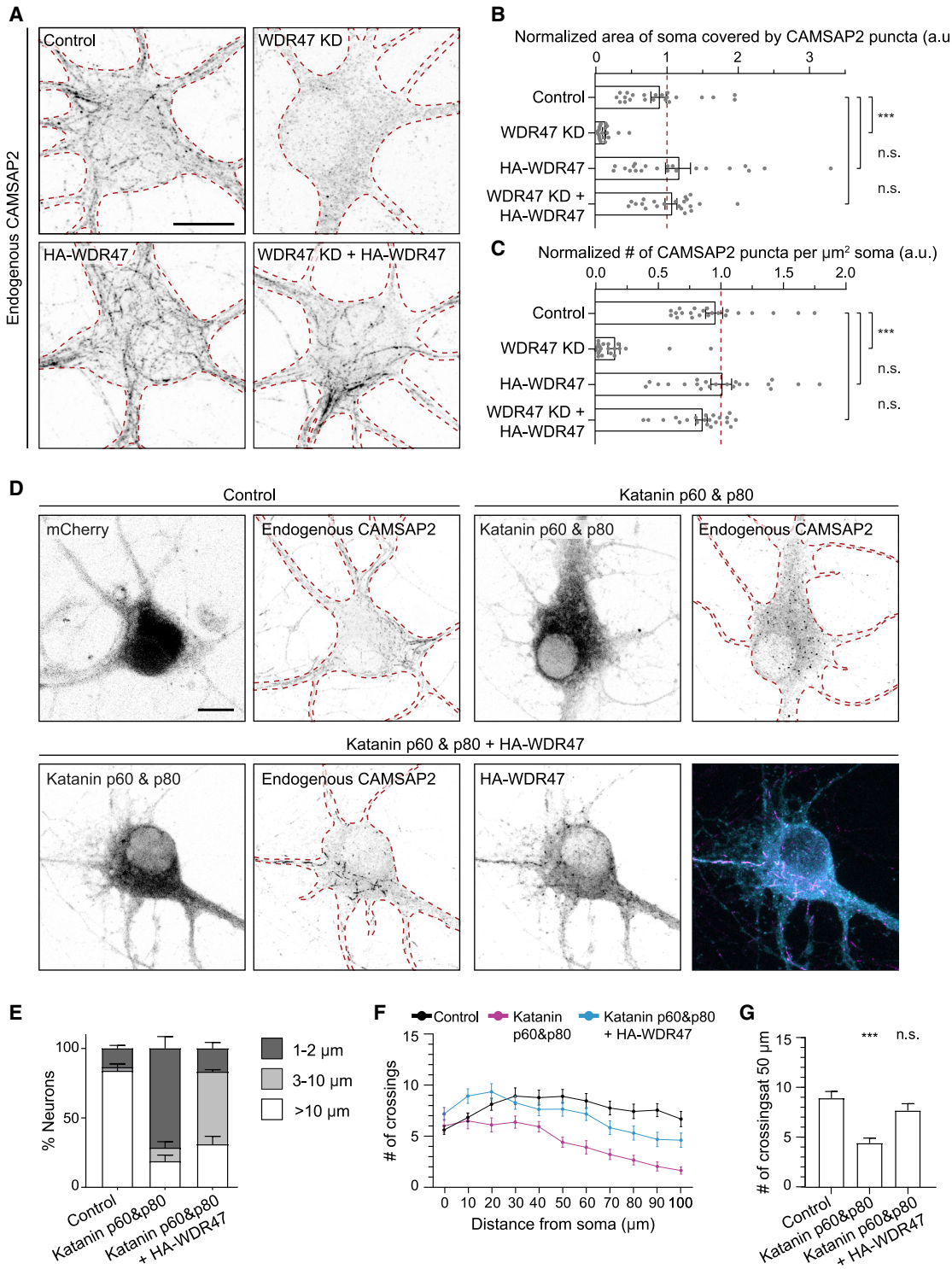

Figure 4. WDR47 protects CAMSAP2 stretches from Katanin

(A) Maximum-intensity projections of CAMSAP2 immunostaining in DIV8 hippocampal neurons co-transfected for 96 h with MARCKS-tagRFP and pSuper control, WDR47 KD, HA-WDR47 or WDR47 KD, and HA-WDR47. Cell outlines are indicated with red dashed lines.

(B) Normalized area of somata covered by CAMSAP2 signal; see also (A). Data were normalized to non-transfected (NT) neurons within the same coverslip, indicated by the red dashed line (N = 3, n = 21–22 and n = 15 for NT neurons).

(legend continued on next page)

additional CAMSAP2 molecules. This may explain the marked colocalization of WDR47 and CAMSAPs in mature neurons, which contain CAMSAP2 stretches with increased length. Future studies using *in-vitro*-reconstituted systems could further characterize the potential positive feedback mechanism and investigate the role of additional components.

WDR47 prevents katanin-mediated severing of MT minus ends

Katanin was identified as a factor that restricts the length of CAMSAP-decorated MT stretches, possibly by cutting MTs or depolymerizing them from the ends (Jiang et al., 2014). Exactly how katanin limits the length of CAMSAP stretches remains to be elucidated. Our results confirm the cutting function of katanin in neurons because we observed significant loss of CAMSAP2 stretches upon katanin expression (Figure 4). Interestingly, the addition of WDR47 prevents the effect of katanin activity on endogenous CAMSAP2 stretches in neurons. Our biochemical data suggest that the WDR47-binding region of CAMSAP2 overlaps with the previously reported katanin-binding helix (Jiang et al., 2018). Therefore, we hypothesize that both proteins compete for interaction with CAMSAP2. However, future work will be needed to determine the exact mode of action.

Based on our findings, we propose that WDR47 is a critical component of the regulatory mechanism mediating MT minus end dynamics. In short, CAMSAP2 binds to and stabilizes MT minus ends. WDR47 interacts with CAMSAP2 and is recruited at the CAMSAP2-decorated MT minus end. Over time, the CAMSAP stretch grows profoundly in neurons, and more WDR47 is recruited. CAMSAP2-limiting factors, such as katanin, are hindered by WDR47, which preserves the structural maintenance and stability of CAMSAP2-positive MT stretches. Lack of WDR47 in neuronal cells leads to loss of stabilized non-centrosomal MT minus ends, which is consistent with the robust brain developmental phenotype observed in WDR47 knockout mice.

STAR★METHODS

Detailed methods are provided in the online version of this paper and include the following:

- KEY RESOURCES TABLE
- RESOURCE AVAILABILITY
  - Lead contact
  - Materials availability
  - Data and code availability
- EXPERIMENTAL MODEL AND SUBJECT DETAILS
  - Animals
  - Heterologous cell culture and transfection
  - Primary neuronal cultures, electroporation and transfection
- METHOD DETAILS
  - DNA, shRNA and CRISPR KI constructs
  - Antibodies
  - Pulldown assays
  - Western blot
  - Affinity Purification-Mass Spectrometry
  - Immunofluorescence fixation and staining
  - Microscopy
- QUANTIFICATION AND STATISTICAL ANALYSIS
  - Statistical analysis
  - Mass spectrometry analysis
  - Image analysis and quantification

SUPPLEMENTAL INFORMATION

Supplemental information can be found online at https://doi.org/10.1016/j.celrep.2021.109371.

ACKNOWLEDGMENTS

We thank Prof. K. Jiang (Wuhan University, China) and Dr. G. Farías (Utrecht University, the Netherlands) for sharing DNA constructs. This work was supported by the Netherlands Organization for Scientific Research (NWO-ALW-VICI to C.C.H. and NWO Graduate Program to R.R.B. [022.003.003]), the Netherlands Organization for Health Research and Development (ZonMW-TOP to C.C.H.) and the European Research Council (ERC) (ERC-consolidator to C.C.H.).

AUTHOR CONTRIBUTIONS

R.R.B. designed and performed experiments, analyzed data, and wrote the manuscript. J.J.A.H. cloned constructs, performed pull-down experiments, and edited the manuscript. M.B. performed COS-7 experiments, analyzed data, and edited the manuscript. X.P. and Y.C. generated CRISPR KI constructs and performed experiments. R.S. performed the mass spectrometry experiment. M.A. supervised the mass spectrometry experiment. A.A. gave advice. L.C.K. supervised the COS-7 experiments. C.C.H. designed and supervised the research and wrote and edited the manuscript.

DECLARATION OF INTERESTS

C.C.H. is an employee of Genentech, Inc., a member of the Roche group.

Received: September 23, 2020
Revised: February 17, 2021
Accepted: June 18, 2021
Published: July 13, 2021

(C) Normalized number of CAMSAP2 puncta detected per μm^2 soma; see also (A). Particles of less than 0.05 μm^2 were excluded from analysis. Data were normalized to NT neurons within the same coverslip (N = 3, n = 21–22 and n = 15 for NT neurons).
(D) Maximum-intensity projections of DIV10 hippocampal neurons co-transfected for 48 h with the transfection marker BFP (data not shown), and mCherry, mCherry-kataninP60&p80 or mCherry-kataninP60&p80 and HA-WDR47 (magenta), stained for CAMSAP2 (cyan). Cell outlines are indicated with red dashed lines.
(E) Quantification of CAMSAP2 staining pattern per condition (see also D), categorized according to Figure S3B (N = 2–3, n = 91–178).
(F) Sholl analysis of DIV10 hippocampal neurons co-transfected for 48 h with GFP and mCherry, mCherry-kataninP60&p80, or mCherry-kataninP60&p80 and HA-WDR47 (N = 2, n = 20).
(G) Average number of crossings at 50-μm distance from the soma; see also (F) (N = 2, n = 20).
Graphs represent mean ± SEM. ***$p < 0.001$. See also Figure S4 and Table S1. Scale bars, 10 μm.

REFERENCES

Abràmoff, M.D., Magalhães, P.J., and Ram, S.J. (2004). Image processing with imageJ. Biophoton. Int. *11*, 36–41.

Akhmanova, A., and Hoogenraad, C.C. (2005). Microtubule plus-end-tracking proteins: mechanisms and functions. Curr. Opin. Cell Biol. *17*, 47–54.

Akhmanova, A., and Hoogenraad, C.C. (2015). Microtubule minus-end-targeting proteins. Curr. Biol. *25*, R162–R171.

Akhmanova, A., and Steinmetz, M.O. (2008). Tracking the ends: a dynamic protein network controls the fate of microtubule tips. Nat. Rev. Mol. Cell Biol. *9*, 309–322.

Akhmanova, A., and Steinmetz, M.O. (2015). Control of microtubule organization and dynamics: two ends in the limelight. Nat. Rev. Mol. Cell Biol. *16*, 711–726.

Baines, A.J., Bignone, P.A., King, M.D., Maggs, A.M., Bennett, P.M., Pinder, J.C., and Phillips, G.W. (2009). The CKK domain (DUF1781) binds microtubules and defines the CAMSAP/ssp4 family of animal proteins. Mol. Biol. Evol. *26*, 2005–2014.

Brummelkamp, T.R., Bernards, R., and Agami, R. (2002). A system for stable expression of short interfering RNAs in mammalian cells. Science *296*, 550–553.

Cao, Y., Lipka, J., Stucchi, R., Burute, M., Pan, X., Portegies, S., Tas, R., Willems, J., Will, L., MacGillavry, H., et al. (2020). Microtubule Minus-End Binding Protein CAMSAP2 and Kinesin-14 Motor KIFC3 Control Dendritic Microtubule Organization. Curr. Biol. *30*, 899–908.e6.

Chen, Y., Zheng, J., Li, X., Zhu, L., Shao, Z., Yan, X., and Zhu, X. (2020). Wdr47 Controls Neuronal Polarization through the Camsap Family Microtubule Minus-End-Binding Proteins. Cell Rep. *31*, 107526.

Conde, C., and Cáceres, A. (2009). Microtubule assembly, organization and dynamics in axons and dendrites. Nat. Rev. Neurosci. *10*, 319–332.

Cunha-Ferreira, I., Chazeau, A., Buijs, R.R., Stucchi, R., Will, L., Pan, X., Adolfs, Y., van der Meer, C., Wolthuis, J.C., Kahn, O.I., et al. (2018). The HAUS Complex Is a Key Regulator of Non-centrosomal Microtubule Organization during Neuronal Development. Cell Rep. *24*, 791–800.

Dammermann, A., Desai, A., and Oegema, K. (2003). The minus end in sight. Curr. Biol. *13*, R614–R624.

Driegen, S., Ferreira, R., van Zon, A., Strouboulis, J., Jaegle, M., Grosveld, F., Philipsen, S., and Meijer, D. (2005). A generic tool for biotinylation of tagged proteins in transgenic mice. Transgenic Research *14*, 477–482.

Farías, G.G., Guardia, C.M., De Pace, R., Britt, D.J., and Bonifacino, J.S. (2017). BORC/kinesin-1 ensemble drives polarized transport of lysosomes into the axon. Proc. Natl. Acad. Sci. USA *114*, E2955–E2964.

Ferreira, T., Blackman, A.V., Oyrer, J., Jayabal, S., Chung, A.J., Watt, A.J., Sjöström, P.J., and van Meyel, D.J. (2014). Neuronal morphometry directly from bitmap images PSFj: Know your fluorescence microscope. Nat. Methods *11*, 981–982.

Goodwin, S.S., and Vale, R.D. (2010). Patronin regulates the microtubule network by protecting microtubule minus ends. Cell *143*, 263–274.

Goslin, K., and Banker, G. (1989). Experimental observations on the development of polarity by hippocampal neurons in culture. J. Cell Biol. *108*, 1507–1516.

Harterink, M., da Silva, M.E., Will, L., Turan, J., Ibrahim, A., Lang, A.E., van Battum, E.Y., Pasterkamp, R.J., Kapitein, L.C., Kudryashov, D., et al. (2017). DeActs: genetically encoded tools for perturbing the actin cytoskeleton in single cells. 14, 479–482.

Hartman, J.J., Mahr, J., McNally, K., Okawa, K., Iwamatsu, A., Thomas, S., Cheesman, S., Heuser, J., Vale, R.D., and McNally, F.J. (1998). Katanin, a Microtubule-Severing Protein, Is a Novel AAA ATPase that Targets to the Centrosome Using a WD40-Containing Subunit. Cell *93*, 277–287.

Hendershott, M.C., and Vale, R.D. (2014). Regulation of microtubule minus-end dynamics by CAMSAPs and Patronin. Proc. Natl. Acad. Sci. USA *111*, 5860–5865.

Jiang, K., Hua, S., Mohan, R., Grigoriev, I., Yau, K.W., Liu, Q., Katrukha, E.A., Altelaar, A.F., Heck, A.J., Hoogenraad, C.C., and Akhmanova, A. (2014). Microtubule minus-end stabilization by polymerization-driven CAMSAP deposition. Dev. Cell *28*, 295–309.

Jiang, K., Rezabkova, L., Hua, S., Liu, Q., Capitani, G., Altelaar, A.F.M., Heck, A.J.R., Kammerer, R.A., Steinmetz, M.O., and Akhmanova, A. (2017). Microtubule minus-end regulation at spindle poles by an ASPM-katanin complex. Nat. Cell Biol. *19*, 480–492.

Jiang, K., Faltova, L., Hua, S., Capitani, G., Prota, A.E., Landgraf, C., Volkmer, R., Kammerer, R.A., Steinmetz, M.O., and Akhmanova, A. (2018). Structural Basis of Formation of the Microtubule Minus-End-Regulating CAMSAP-Katanin Complex. Structure *26*, 375–382.e4.

Kannan, M., Bayam, E., Wagner, C., Rinaldi, B., Kretz, P.F., Tilly, P., Roos, M., McGillewie, L., Bär, S., Minocha, S., et al. (2017). WD40-repeat 47, a microtubule-associated protein, is essential for brain development and autophagy. Proc. Natl. Acad. Sci. USA *114*, E9308–E9317.

Kapitein, L.C., and Hoogenraad, C.C. (2015). Building the Neuronal Microtubule Cytoskeleton. Neuron *87*, 492–506.

Kapitein, L.C., Schlager, M.A., van der Zwan, W.A., Wulf, P.S., Keijzer, N., and Hoogenraad, C.C. (2010a). Probing intracellular motor protein activity using an inducible cargo trafficking assay. Biophys. J. *99*, 2143–2152.

Kapitein, L.C., Yau, K.W., and Hoogenraad, C.C. (2010b). Microtubule Dynamics in Dendritic Spines. Methods Cell Biol. *97*, 111–132.

Kollman, J.M., Merdes, A., Mourey, L., and Agard, D.A. (2011). Microtubule nucleation by γ-tubulin complexes. Nat. Rev. Mol. Cell Biol. *12*, 709–721.

McNally, F.J., and Vale, R.D. (1993). Identification of katanin, an ATPase that severs and disassembles stable microtubules. Cell *75*, 419–429.

Meijering, E., Jacob, M., Sarria, J.C., Steiner, P., Hirling, H., and Unser, M. (2004). Design and validation of a tool for neurite tracing and analysis in fluorescence microscopy images. Cytometry A *58*, 167–176.

Meng, W., Mushika, Y., Ichii, T., and Takeichi, M. (2008). Anchorage of microtubule minus ends to adherens junctions regulates epithelial cell-cell contacts. Cell *135*, 948–959.

Pongrakhananon, V., Saito, H., Hiver, S., Abe, T., Shioi, G., Meng, W., and Takeichi, M. (2018). CAMSAP3 maintains neuronal polarity through regulation of microtubule stability. Proc. Natl. Acad. Sci. USA *115*, 9750–9755.

Roll-Mecak, A., and McNally, F.J. (2010). Microtubule-severing enzymes. Curr. Opin. Cell Biol. *22*, 96–103.

Schindelin, J., Arganda-Carreras, I., Frise, E., Kaynig, V., Longair, M., Pietzsch, T., Preibisch, S., Rueden, C., Saalfeld, S., Schmid, B., et al. (2012). Fiji: an open-source platform for biological-image analysis. Nat. Methods *9*, 676–682.

Tanaka, N., Meng, W., Nagae, S., and Takeichi, M. (2012). Nezha/CAMSAP3 and CAMSAP2 cooperate in epithelial-specific organization of noncentrosomal microtubules. Proc. Natl. Acad. Sci. USA *109*, 20029–20034.

Teixidó-Travesa, N., Roig, J., and Lüders, J. (2012). The where, when and how of microtubule nucleation - one ring to rule them all. J. Cell Sci. *125*, 4445–4456.

Tortosa, E., Adolfs, Y., Fukata, M., Pasterkamp, R.J., Kapitein, L.C., and Hoogenraad, C.C. (2017). Dynamic Palmitoylation Targets MAP6 to the Axon to Promote Microtubule Stabilization during Neuronal Polarization. Neuron *94*, 809–825.e7.

van Beuningen, S.F.B., Will, L., Harterink, M., Chazeau, A., van Battum, E.Y., Frias, C.P., Franker, M.A.M., Katrukha, E.A., Stucchi, R., Vocking, K., et al. (2015). TRIM46 Controls Neuronal Polarity and Axon Specification by Driving the Formation of Parallel Microtubule Arrays. Neuron *88*, 1208–1226.

van der Vaart, B., van Riel, W.E., Doodhi, H., Kevenaar, J.T., Katrukha, E.A., Gumy, L., Bouchet, B.P., Grigoriev, I., Spangler, S.A., Yu, K.L., et al. (2013). CFEOM1-associated kinesin KIF21A is a cortical microtubule growth inhibitor. Dev. Cell *27*, 145–160.

Wang, W., Lundin, V.F., Millan, I., Zeng, A., Chen, X., Yang, J., Allen, E., Chen, N., Bach, G., Hsu, A., et al. (2012). Nemitin, a Novel Map8/Map1s Interacting Protein with Wd40 Repeats. PLoS One *7*, e33094.

Willems, J., de Jong, A.P.H., Scheefhals, N., Mertens, E., Catsburg, L.A.E., Poorthuis, R.B., de Winter, F., Verhaagen, J., Meye, F.J., and MacGillavry, H.D. (2020). ORANGE: A CRISPR/Cas9-based genome editing toolbox for epitope tagging of endogenous proteins in neurons. PLoS Biol. *18*, e3000665.

Yau, K.W., van Beuningen, S.F., Cunha-Ferreira, I., Cloin, B.M., van Battum, E.Y., Will, L., Schätzle, P., Tas, R.P., van Krugten, J., Katrukha, E.A., et al. (2014). Microtubule minus-end binding protein CAMSAP2 controls axon specification and dendrite development. Neuron *82*, 1058–1073.

Yuan, B., Latek, R., Hossbach, M., Tuschl, T., Lewitter, F., et al. (2004). siRNA selection server: An automated siRNA oligonucleotide predicition server. Nucleic Acids Res. *32*, 130–134.

Zhou, Z., Xu, H., Li, Y., Yang, M., Zhang, R., Shiraishi, A., Kiyonari, H., Liang, X., Huang, X., Wang, Y., et al. (2020). CAMSAP1 breaks the homeostatic microtubule network to instruct neuronal polarity. Proc. Natl. Acad. Sci. USA *117*, 222193–222203.

STAR★METHODS

KEY RESOURCES TABLE

REAGENT or RESOURCE	SOURCE	IDENTIFIER
Antibodies		
mouse anti-Actin	Millipore	Cat# MAB1501; RRID: AB_2223041
mouse anti-Ankyrin-G	UC Davis/NIH NeuroMab Facility	Clone N106/36; Cat# 75-146; RRID: AB_10673030
rabbit anti-CAMSAP2	Proteintech	Cat# 17880-1-AP; RRID: AB_2068826
chicken anti-GFP	Aves Labs,	Cat# GFP-1020; RRID: AB_10000240
mouse anti-GFP	Thermo Fisher Scientific	Clone 3E6; Cat# A-11120; RRID: AB_221568
rabbit anti-GFP	MBL Sanbio	Cat# 598; RRID: AB_591819
rabbit anti-GFP	Abcam	Cat# ab290; RRID: AB_303395
mouse anti-HA	Roche	Clone 12CA5; Cat# 11666606001; RRID: AB_514506
rat anti-HA	Roche	Clone 3F10; Cat# 11867423001; RRID: AB_390918
mouse anti-HA	Covance	Clone 16B12; Cat# MMS-101P-200; RRID: AB_10064068
chicken anti-MAP2	Abcam	Cat# ab5392; RRID: AB_2138153
mouse anti-Pan-Nav	Sigma-Aldrich	Clone K58/35; Cat# S8809; RRID: AB_477552
mouse anti-Tau-1	Millipore	Clone PC1C6; Cat# MAB3420; RRID: AB_94855
rabbit anti-TRIM46	From C. C. Hoogenraad (van Beuningen et al., 2015)	N/A
and rabbit anti-WDR47	Atlas Antibodies	Cat# HPA027287; RRID: AB_10599416
goat anti-chicken Alexa405	Abcam	Cat# ab175675; RRID: AB_2810980
goat anti-chicken Alexa488	Life Technologies	Cat# A-11039; RRID: AB_142924
goat anti-rabbit Alexa647	Life Technologies	Cat# A-21245; RRID: AB_2535813
goat anti-mouse Alexa405	Life Technologies	Cat# A-31553, RRID:AB_221604
goat anti-mouse Alexa488	Life Technologies	Cat# A-11029; RRID: AB_2534088
goat anti-mouse Alexa568	Life Technologies	Cat# A-11031; RRID: AB_144696
goat anti-mouse Alexa647	Life Technologies	Cat# A-21236; RRID: AB_2535805
goat anti-rabbit Alexa488	Life Technologies	Cat# A-11034; RRID: AB_2576217
goat anti-rabbit Alexa568	Life Technologies	Cat# A-11036; RRID: AB_10563566
goat anti-rat Alexa647	Life Technologies	Cat# A-21247; RRID: AB_141778
goat anti-mouse IRDye680LT Conjugated	LI-COR Biosciences	Cat# 926-68020; RRID: AB_10706161
goat anti-mouse IRDye800CW Conjugated	LI-COR Biosciences	Cat# 926-32210; RRID: AB_621842
goat anti-rabbit IRDye680LT Conjugated	LI-COR Biosciences	Cat# 926-68021; RRID: AB_10706309
goat anti-rabbit IRDye 800CW Conjugated	LI-COR Biosciences	Cat# 926-32211; RRID: AB_621843
Chemicals, peptides, and recombinant proteins		
SIR-tubulin	Spiro Chrome	Cat# SC002
FuGENE 6	Promega	Cat# E2692
Lipofectamine 2000	Thermo Fisher Vectorlabs	Cat# 11668019
polyethylenimine (PEI MAX)	PolySciences	Cat# 24765
Critical commercial assays		
Dynabeads M-280 streptavidin beads	Thermo Fisher	Cat# 11206D
Rat Neuron Nucleofector kit (AMAXA)	Lonza	Cat# VVPG-1003

(*Continued on next page*)

Continued

REAGENT or RESOURCE	SOURCE	IDENTIFIER
Experimental models: Cell lines		
Human embryonic kidney 293T (HEK293T)	ATCC	Cat# CRL-3216
African Green Monkey SV40-transformed kidney fibroblast (COS-7)	ATCC	Cat# CRL-1651
Experimental models: Organisms/strains		
Rat (Wistar)	Janvier	N/A
Oligonucleotides		
pSuper rat WDR47 shRNA#3 target sequence: GATCAAACGACAAATATGT	This paper	N/A
CRISPR KI CAMSAP2, guide RNA target sequence: AAGAGTTTTTTGGGTGTCAC	This paper	N/A
CRISPR KI CAMSAP3, guide RNA target sequence: TAGCCCCGGCGTCGCCATGG	This paper	N/A
pSuper rat WDR47 shRNA#1 target sequence: GCTTATTCTGGATGGTCAA	This paper	N/A
pSuper rat WDR47 shRNA#2 target sequence: GCTTATTCCAGCTCGTAAT	This paper	N/A
Recombinant DNA		
pβactin-GFP	Kapitein et al., 2010a	N/A
pBio-GFP vector	van der Vaart et al., 2013	N/A
pGW2-Tag-BFP	Tortosa et al., 2017	N/A
pGW2-mCherry	Cunha-Ferreira et al., 2018	N/A
pGW1-GFP-CAMSAP2	Yau et al., 2014	N/A
pGW1-GFP-CAMSAP3	Yau et al., 2014	N/A
3GFP-CAMSAP2	Cao et al., 2020	N/A
Protein-biotin ligase BirA (3HA-BirA)	Kind gift from Dr. D. Meijer, University of Edinburgh (Driegen et al., 2005)	N/A
plasma membrane marker FYN-FKBP1A-RFP (PM-RFP)	Kind gift from Dr. G. Farías, Utrecht University (Farías et al., 2017)	N/A
pSuper vector	Brummelkamp et al., 2002	N/A
pGW2-GFP-WDR47	This paper	N/A
pGW2-GFP	Cunha-Ferreira et al., 2018	N/A
pGW2-mCherry-WDR47	This paper	N/A
pGW1-HA-WDR47	This paper	N/A
pGW1-HA-CAMSAP1	This paper	N/A
pGW1-HA-CAMSAP2	This paper	N/A
pGW1-HA-CAMSAP3	This paper	N/A
pGW1-HA-CAMSAP2_CC-CH	This paper	N/A
pGW1-HA-CAMSAP2_Middle	This paper	N/A
pGW1-HA-CAMSAP2_2xCC	This paper	N/A
pGW1-HA_MBD-CKK	This paper	N/A
pGW1-HA-WDR47_LisH	This paper	N/A
pGW1-HA-WDR47_Middle	This paper	N/A
pGW1-HA-WDR47_WD40	This paper	N/A
pBio-GFP-WDR47	This paper	N/A
pBio-GFP-CAMSAP2	This paper	N/A
pBio-GFP-CAMSAP2_Middle	This paper	N/A
pGW1-mCherry-katanin p60	This paper	N/A
pGW1-mCherry-katanin p80	This paper	N/A
pGW2-MARCKS-TagRFP-T	Harterink et al., 2017	N/A

(*Continued on next page*)

Continued

REAGENT or RESOURCE	SOURCE	IDENTIFIER
Software and algorithms		
NeuronJ plugin for ImageJ/Fiji	Meijering et al., 2004	RRID: SCR_002074
Fiji	Schindelin et al., 2012	RRID: SCR_002285
Sholl Analysis plugin for ImageJ/Fiji	Ferreira et al., 2014	https://fiji.sc/Sholl
ComDet plugin for ImageJ/Fiji	GitHub	https://github.com/ekatrukha/ComDet
ImageJ	Abràmoff et al., 2004	RRID: SCR_003070

RESOURCE AVAILABILITY

Lead contact

Further information and requests for resources and reagents should be directed to and will be fulfilled by the Lead Contact, Casper Hoogenraad (c.hoogenraad@uu.nl).

Materials availability

Plasmids generated in this study are available on request.

Data and code availability

The published article includes all datasets analyzed in this study.

EXPERIMENTAL MODEL AND SUBJECT DETAILS

Animals

All animal experiments were performed in compliance with institutional guidelines of Utrecht University, in agreement the guidelines for the welfare of experimental animals issued by the Federal Government of the Netherlands and European regulations (Directive 2010/63/EU) and approved by the Dutch Animal Experiments Review Committee (Dier Experimenten Commissie; license AVD1080020173404).

Female pregnant Wistar rats (Janvier) were at least 10 weeks old and not involved in previous experiments. The animals were housed with companions in transparent plexiglas cages with wood-chip bedding and paper tissue for nest building and cage enrichment. They were kept in a controlled 12 h light-dark cycle with a temperature of 22 ± 1°C and were given unrestricted access to food and water. Hippocampal and cortical neurons were obtained from embryos of both genders at E18 stage of development. None of the parameters analyzed in this study are reported to be affected by embryo gender.

Heterologous cell culture and transfection

Human embryonic kidney 293T (HEK293T) and African Green Monkey SV40-transformed kidney fibroblast (COS-7) cells were from American Type Culture Collection (ATCC). Cell lines were not authenticated by authors after purchase and regularly checked for mycoplasma contamination using Mycoalert detection kit (Lonza).

HEK293T cells were cultured in 50/50 DMEM/Ham's F10 medium (Lonza), supplemented with 10% fetal calf serum (FCS; Sigma) and 1% penicillin/streptomycin (Sigma) at 37°C and 5% CO_2. Cells were seeded into 6-well plates and transfected after 24 hr using polyethylenimine (PEI MAX, PolySciences) according to manufacturer's protocol. Briefly, PEI (1 μg/μL): DNA (1 μg/μL) (3:1) were mixed in Ham's F10 and incubated at room temperature for 20 minutes, after which the mixture was added to the cells and incubated for 24 hr.

COS-7 cells were cultured in DMEM supplemented with 10% FCS and 1% penicillin/streptomycin at 37°C and 5% CO_2. Cells were seeded onto 24mm glass coverslips in a 6-well plate and transfected after 24 hr using FuGENE6 transfection reagent (Promega). Briefly, FuGENE6: DNA (μg/μL) (3:1 vol) were mixed in Opti-MEM medium (GIBCO) and incubated for 5 minutes at room temperature, after which the mixture was added to the cells. SiR-tubulin (Spirochrome) was added to the complete medium at 100nM concentration 3-4 hr prior to imaging to visualize microtubules. Cells were imaged 16-24 hr after transfection.

Primary neuronal cultures, electroporation and transfection

Primary hippocampal and cortical cultures were prepared from E18 rat brains (both genders) by mechanical and enzymatic dissociation (Goslin and Banker, 1989; Kapitein et al., 2010b). Hippocampal neurons were plated on 18mm glass coverslips coated with poly-L-lysine (37.5 μg/mL, Sigma) and laminin (1.25 μg/mL, Roche Diagnostics) at a density of 100,000 cells/well in a 12-well plate. Neurons were cultured in Neurobasal medium (NB; GIBCO) supplemented with 2% B27 (GIBCO), 0.5 mM glutamine (GIBCO), 15.6 μM glutamate (Sigma), and 1% penicillin/ streptomycin (GIBCO) at 37°C in 5% CO2.

For electroporation, hippocampal and cortical neurons were collected directly after dissection and dissociation, centrifuged for 5 minutes at 200 g and resuspended in AMAXA solution (Lonza). For each sample neurons were mixed with DNA, transferred to a gene pulser cuvette (Biorad) and electroporated using a Lonza Nucleofector 2b. For biochemistry experiments cortical neurons were used ($1.2*10^6$ cells and 3μg of DNA per sample in 6-well plates) and grown for 96 hr prior to lysis and western blot analysis. For imaging experiments hippocampal neurons were used ($1,75*10^5$ cells and ~1μg of DNA per sample in 12-well plates) and grown for 48-96 hr prior to fixation and immunocytochemistry. Electroporation of hippocampal neurons was used for datasets shown in Figures S1E–S1I.

Neuron transfections were done on hippocampal neurons using Lipofectamine 2000 (Invitrogen) according to manufacturer's protocol. In short, for each well 1-2 μg DNA was mixed with 3.3 μL of Lipofectamine 2000 in 200 μL NB and incubated for 30 minutes. The neuronal growth medium was temporarily removed from the wells and replaced by NB supplemented with 0.5 mM glutamine, to which the DNA mix was added for 45 minutes to 1 hr. Afterward, neurons were washed with NB and transferred back into their original medium for 24-48 hr (for overexpression) or 96 hr (for shRNA expression).

METHOD DETAILS

DNA, shRNA and CRISPR KI constructs

The following mammalian expression vectors have been described before: pGW2-GFP (Cunha-Ferreira et al., 2018), pGW2-MARCKS-TagRFP-T (Harterink et al., 2017), pβactin-GFP (Kapitein et al., 2010a), pBio-GFP vector (van der Vaart et al., 2013), pGW2-Tag-BFP (Tortosa et al., 2017), pGW2-mCherry (Cunha-Ferreira et al., 2018), pGW1-GFP-CAMSAP2 and pGW1-GFP-CAMSAP3 (Yau et al., 2014), however 3GFP-CAMSAP2 (Cao et al., 2020) was used for live imaging experiments. The biotin ligase BirA expression construct was a kind gift from Dr. D. Meijer (University of Edinburgh, UK) and contains a triple hemagglutinin (HA)-tag (Driegen et al., 2005). The plasma membrane marker construct PM-RFP was a kind gift from Dr. G. Farías (Utrecht University, the Netherlands) (Farías et al., 2017).

Full length human WDR47 (cDNA clone MGC:26714 IMAGE:4823902; clone accession GenBank: BC034964), in which two point mutations were detected (A2599G and T2630C) was repaired to match the sequence of the human genome (Ensembl: ENSG00000085433 and CCDS: CCDS30787). To generate pGW2-GFP-WDR47, pGW2-mCherry-WDR47 and pGW1-mHA-WDR47 the full length WDR47 was amplified by PCR and inserted into AscI/SalI restriction sites of the pGW2-GFP, pGW1-HA and pGW2-mCherry vectors (Cunha-Ferreira et al., 2018). HA-tagged CAMSAP1/2/3 constructs were generated by PCR based strategies using previously described pGW1-GFP-CAMSAP1 (human), pGW1-GFP-CAMSAP2 (human) and pGW1-GFP-CAMSAP3 (mouse) (Yau et al., 2014) as templates and ligation into the pGW1-HA backbone. Truncated CAMSAP2 constructs were generated using PCR based strategies with pGW1-HA-CAMSAP2 as template and pGW1-HA as backbone to result in pGW1-HA-CAMSAP2_CC-CH, pGW1-HA-CAMSAP2_Middle, pGW1-HA-CAMSAP2_2xCC, and pGW1-HA_MBD-CKK. Truncated WDR47 constructs were generated using PCR based strategies with pGW1-HA-WDR47 as template and pGW1-HA as backbone to result in pGW1-HA-WDR47_LisH, pGW1-HA-WDR47_Middle, pGW1-HA-WDR47_WD40, pGW1-HA-WDR47_N, and pGW1-HA-WDR47_C. pBio-GFP-WDR47, pBio-GFP-WDR47_N, and pBio-GFP-WDR47_C were cloned using a PCR based strategy with GW1-HA-WDR47 as template and ligation into the pBio-GFP backbone. pBio-GFP-CAMSAP2 and pBio-GFP-CAMSAP2_Middle were created with a similar strategy using pGW1-HA-CAMSAP2 as template. pGW1-mCherry-katanin p60 and pGW1-mCherry-katanin p80 were generated using PCR based strategies to insert mouse katanin p60 and p80, which were a kind gift from Prof. K. Jiang (Wuhan University, China) (Jiang et al., 2017), into mCherry backbone.

The shRNA constructs were created using pSuper vector (Brummelkamp et al., 2002), which was also used as control. The following target sequences were used in this study: pSuper rat WDR47 shRNA#1 (WDR47 KD#1, 5′- GCTTATTCTGGATGGTCAA −3′), pSuper rat WDR47 shRNA#2 (WDR47 KD#2, 5′- GCTTATTCCAGCTCGTAAT −3′), pSuper rat WDR47 shRNA#3 (WDR47 KD#3, 5′- GATCAAACGACAAATATGT −3′). These shRNA sequences were created to target rat WDR47 (Ensembl: ENSRNOT00000055862.2 and GenBank: NM_ 001100702.1) using http://sirna.wi.mit.edu/ (Yuan et al., 2004). The complementary oligonucleotides were annealed and inserted in the pSuper vector with HindIII/BglII restriction enzymes. The rat WDR47 shRNAs generated in this study do not target the human WDR47 allowing the use of human WDR47 overexpression constructs for rescue experiments.

The CRISPR knock-in constructs were created using pORANGE vector (Willems et al., 2020). Guide RNAs for CAMSAP2 and CAMSAP3 were designed using the *CRISPR Guide RNA Design Tool* from Benchling. The targeting sequences for guide RNAs were as follows: CAMSAP2: 5′-AAGAGTTTTTTGGGTGTCAC-3′, CAMSAP3: 5′-TAGCCCCGGCGTCGCCATGG-3′.

Antibodies

The following primary antibodies were used in this study: mouse anti-Actin (Millipore, Cat# MAB1501, RRID: AB_2223041), mouse anti-Ankyrin-G, clone N106/36 (UC Davis/NIH NeuroMab Facility, Cat# 75-146, RRID: AB_10673030), rabbit anti-CAMSAP2 (Proteintech, Cat# 17880-1-AP, RRID: AB_2068826), for immunocytochemistry chicken anti-GFP (Aves Labs, Cat# GFP-1020, RRID: AB_10000240), mouse anti-GFP, clone 3E6 (Thermo Fisher Scientific, Cat# A-11120, RRID: AB_221568) and rabbit anti-GFP (MBL Sanbio, Cat# 598, RRID: AB_591819), for western blot rabbit anti-GFP (Abcam, Cat# ab290, RRID: AB_303395), for immunocytochemistry mouse anti-HA, clone 12CA5 (Roche, Cat# 11666606001, RRID: AB_514506) and rat anti-HA, clone 3F10 (Roche,

Cat# 11867423001, RRID: AB_390918), for western blot mouse anti-HA, clone 16B12 (Covance, Cat# MMS-101P-200, RRID: AB_10064068), chicken anti-MAP2 (Abcam, Cat# ab5392, RRID: AB_2138153), mouse anti-Pan-Nav, clone K58/35 (Sigma-Aldrich, Cat# S8809, RRID: AB_477552), mouse anti-Tau-1, clone PC1C6 (Millipore, Cat# MAB3420, RRID: AB_94855), rabbit anti-TRIM46 (homemade; van Beuningen et al., 2015) and rabbit anti-WDR47 (Atlas Antibodies, Cat# HPA027287, RRID: AB_10599416).

The following secondary antibodies were used in this study: for immunofluorescence we used goat anti-chicken Alexa405 (Abcam Cat# ab175675, RRID: AB_2810980), goat anti-chicken Alexa488 (Life Technologies, Cat# A-11039, RRID: AB_142924), goat anti-mouse Alexa405 (Life Technologies, Cat# A-31553, RRID: AB_221604), goat anti-mouse Alexa488 (Life Technologies, Cat# A-11029, RRID: AB_2534088), goat anti-mouse Alexa568 (Life Technologies, Cat# A-11031, RRID: AB_144696), goat anti-mouse Alexa647 (Life Technologies, Cat# A-21236, RRID: AB_2535805), goat anti-rabbit Alexa488 (Life Technologies, Cat# A-11034, RRID: AB_2576217), goat anti-rabbit Alexa568 (Life Technologies, Cat# A-11036, RRID: AB_10563566), goat anti-rabbit Alexa647 (Life Technologies, Cat# A-21245, RRID: AB_2535813) and goat anti-rat Alexa647 (Life Technologies, Cat# A-21247, RRID: AB_141778). For western blotting we used goat anti-mouse IRDye680LT Conjugated (LI-COR Biosciences, Cat# 926-68020, RRID: AB_10706161), goat anti-mouse IRDye800CW Conjugated (LI-COR Biosciences, Cat# 926-32210, RRID: AB_621842), goat anti-rabbit IRDye680LT Conjugated (LI-COR Biosciences, Cat# 926-68021, RRID: AB_10706309) and goat anti-rabbit IRDye 800CW Conjugated (LI-COR Biosciences, Cat# 926-32211, RRID: AB_621843).

Pulldown assays

Streptavidin pulldown assays were performed on HEK293T cell lysates by co-expressing biotin ligase BirA with Bio-GFP constructs (bait) and HA-tagged constructs (prey) using polyethylenimine (PEI MAX, PolySciences) according to manufacturer's protocol. 24 hr after transfection, cells were washed in ice-cold PBS and lysed for 30 minutes on ice in lysis buffer (100 mM TrisHCl pH 7.5, 150 mM NaCl, 1% Triton X-100, protease inhibitors (Roche)). Lysates were then cleared by centrifugation for 15 minutes at 13.2 krpm at 4°C. Supernatants were collected and incubated with blocked (incubation for 30 minutes at RT in 50 mM Tris–HCl pH 7.5, 150 mM KCl, 0.2 μg/μl chicken egg albumin) Streptavidin Dynabeads M-280 (Invitrogen) for 1.5 hr at 4°C. Beads were washed five times with washing buffer (100 mM Tris–HCl pH 7.5, 250 mM NaCl, 0.5% Triton X-100). Finally, proteins were eluded by boiling the beads for 10 minutes at 95°C in 2x DTT+ sample buffer (20% glycerol, 4% SDS, 200 mM DTT, 100 mM Tris–HCl pH 6.8, bromophenol blue) and analyzed by western blotting.

Western blot

For shRNA validation and WDR47 expression levels, cortical neuron lysates were prepared at indicated DIVs by quickly washing the neurons in ice-cold PBS and collecting them by scraping directly in DTT+ sample buffer (4% SDS, 20% glycerol, 100 mM Tris pH 6.8, 200 mM DTT and 20 mg/l bromophenol blue). Samples were boiled for 10 minutes at 99°C and centrifuged at 13.2 krpm for 10 minutes before being analyzed on 10% SDS-PAGE gels. For pulldown experiments, collected protein samples were ran on either 6% SDS-PAGE gels or 6%–14% SDS-PAGE gradient gels. Proteins were transferred to nitrocellulose membranes (Bio-Rad) using a semi-dry or wet blotting system (Bio-Rad).

Next, membranes were incubated in 3% bovine serum albumin (BSA) in PBST (PBS supplemented with 0.02% Tween20) for 1 hr at room temperature, which was followed by incubation with primary antibodies in 3% BSA-PBST at 4°C overnight. Membranes were washed three times with PBST, before incubation with secondary antibody in 3% BSA-PBST for 1 hr at room temperature, and another three washes with PBST. Blots were acquired using an Odyssey Infrared Imaging system (LI-COR Biosciences) and scanned at 680 nm and 800 nm.

Affinity Purification-Mass Spectrometry

Streptavidin beads pulldown assays were performed with HEK293 cells transfected with Bio-GFP-WDR47 or Bio-GFP together with BirA using polyethylenimine (PEI MAX, PolySciences) for 48 hr according to the manufacturer's instructions. Cells were lysed in RIPA lysis buffer (50 mM TrisHCl pH 7.4-7.8, 150 mM NaCl, 1% Triton X-100, 0.1% SDS, 0.5% Sodium Deoxycholate) and Protease inhibitors (Roche) for 30 minutes and centrifuged at 13.2 krpm for 15 minutes at 4°C. The supernatants were incubated with Dynabeads M-280 (pre-blocked for 30 minutes at room temperature in 20 mM Tris–HCl pH 7.5, 150 mM KCl, 0.2 μg/μl chicken egg albumin) for 1 hr at 4°C. The beads were separated using a magnet rack (Dynal, Invitrogen).

To sample for brain interactors of WDR47, beads pre-incubated with HEK293 cell extracts expressing the constructs were washed twice in low salt washing buffer (20 mM Tris-HCl pH 7.4-7.8, 100 mM KCl, 0.1% Triton X-100), followed by two wash steps in high salt wash buffer (20 mM Tris-HCl pH 7.4-7.8, 500 mM KCl, 0.1% Triton X-100) and two final wash steps in low salt washing buffer to remove binding proteins from HEK293 cells. Brains were obtained from female adult rats and homogenized in 10x volume/weight in tissue lysis buffer (50 mM TrisHCl, 150 mM NaCl, 0.1% SDS, 0.2% NP-40, and protease inhibitors (Roche)). Brain lysates were centrifuged at 13.2 krpm for 10 minutes at 4°C and the supernatant was incubated with the beads containing Bio-GFP-WDR47 or Bio-GFP for 2 hr at 4°C and washed in normal washing buffer five times.

To prepare for mass spectrometry analysis, beads were resuspended in 15 μL of 4x Laemmli sample buffer (Bio-Rad) and supernatants were loaded on a 4%–12% gradient Criterion XT Bis-Tris precast gel (Bio-Rad). The gel was fixed with 40% methanol and

10% acetic acid and then stained for 1 hr using colloidal Coomassie dye G-250 (Gel Code Blue Stain Reagent, Thermo Scientific). Samples were then subjected to in gel-digestion using trypsin, as described previously (Cunha-Ferreira et al., 2018).

Immunofluorescence fixation and staining

For immunocytochemistry that included WDR47 or CAMSAP2 antibodies, neurons were fixed for 2 minutes with methanol (100%) at −20°C followed by 8 minutes with paraformaldehyde (4%) plus sucrose (4%) at room temperature. For all other immunocytochemistry experiments neurons were fixed for 10 minutes with paraformaldehyde (4%) plus sucrose (4%) at room temperature.

Fixed neurons were washed 3 times with PBS and incubated with primary antibodies in GDB buffer (0.2% BSA, 0.8 M NaCl, 0.5% Triton X-100, 30 mM phosphate buffer, pH 7.4) overnight at 4°C. After 3 times washing with PBS, cells were incubated with secondary antibodies in GDB buffer for 1 hr at room temperature. After washing, coverslips were mounted in Vectashield (VectorLabs).

For immunocytochemistry experiments with electroporated neurons (datasets shown in Figure S1E-I) a quicker protocol was used. The fixed neurons were first washed 3 times with PBS-CM (PBS, 1 mM $MgCl_2$, 0.1 mM $CaCl_2$), next permeabilized for 15 minutes with 0.2% Triton X-100 followed by blocking with 0.2% gelatin for 30 min at 37°C. Then, coverslips were incubated for 30 minutes at 37°C with primary antibodies diluted in 0.2% gelatin, washed 3 times with PBS-CM and incubated with secondary antibodies, again for 30 minutes at 37°C. After washing 3 times in PBS-CM, coverslips were mounted in Fluoromount (Invitrogen).

Microscopy

For axon morphology images of fixed cells were collected with a wide-field fluorescence microscope Nikon Eclipse 80i equipped with C-HGFI Fiber Illuminator "Intensilight" (Nikon), Plan Fluor 20x N.A. 0.75 oil objective (Nikon) and ET-DAPI (49000, Chroma), ET-GFP (49002, Chroma), ET-mCherry (49008, Chroma) filters, CoolSNAP HQ2 CCD camera (Photometrics) and NIS-Elements Br software (Nikon). All other fixed experiments were imaged using a confocal fluorescence microscope LSM 700 (Zeiss) equipped with a Plan-Apochromat 63x/1.40 oil objective (Zeiss) using ZEN2011 software.

Live imaging of neurons (image shown in Figure S1A) was performed by spinning disk confocal microscopy on inverted research microscope Nikon Eclipse Ti-E (Nikon), equipped with the perfect focus system (Nikon) Nikon Plan Apo 60x N.A. 1.40 oil objective (Nikon) and a spinning disk-based confocal scanner unit (CSU-X1-A1, Yokogawa). The system was also equipped with ASI motorized stage with the piezo plate MS-2000-XYZ (ASI), Photometrics Evolve Delta 512 EMCCD camera (Photometrics) and controlled by the MetaMorph 7.8 software (Molecular Devices). 491nm 100mW Calypso (Cobolt) laser was used as the light sources. We used ET-GFP filter set (49002, Chroma) for imaging of proteins tagged with GFP; 16-bit images were projected onto the EMCCD chip with intermediate lens 2.0X (Edmund Optics) at a magnification of 111 μm/pixel. To keep cells at 37°C we used stage top incubator (model INUBG2E-ZILCS, Tokai Hit). Coverslips were mounted in a Ludin chamber (life imaging services).

Live imaging of COS-7 cells was performed using an Azimuthal spinning TIRFM on an inverted research microscope Nikon Eclipse Ti-E (Nikon), equipped with the perfect focus system (Nikon), Nikon Apo TIRF 100x N.A. 1.49 oil objective (Nikon) and iLas2 system (Dual Laser illuminator for azimuthal spinning TIRF (or Hilo) illumination and Simultaneous Targeted Laser Action) from Roper Scientific (Evry, France; now Gataca Systems) with a custom modification for targeted Photoablation using a 532 nm pulsed laser. The system was also equipped with ASI motorized stage MS-2000-XY (ASI), Photometrics Evolve Delta 512 EMCCD camera (Photometrics) and controlled by the MetaMorph 7.8 software (Molecular Devices). Stradus 488 nm (150 mW, Vortran), OBIS 561 nm (100 mW, Coherent) and Stradus 642 nm (110 mW, Vortran) lasers were used as light sources. We used ET-GFP filter set (49002, Chroma) for imaging of proteins tagged with GFP; ET-mCherry filter set (49008, Chroma) for imaging of proteins tagged with mCherry and ET-Cy5 filter set (49006, Chroma) for imaging far-red dyes. 16-bit images were projected onto the EMCCD chip with intermediate lens 2.5X (Nikon C mount adaptor 2.5X) at a magnification of 0.065 μm/pixel for microtubule severing experiments. To keep cells at 37°C we used stage top incubator (model INUBG2E-ZILCS, Tokai Hit). Coverslips were mounted in AttoFluor cell chamber (ThermoFischer) and sealed with coverslip on top. For microtubule severing experiments, individual microtubules at the cell periphery were severed with a 532nm Q-switched pulsed laser (Teem Photonics) and then imaged with 7 s interval for total 4-5 minutes to track CAMSAP2 and WDR47 localization at microtubule minus end.

QUANTIFICATION AND STATISTICAL ANALYSIS

Statistical analysis

All statistical details including the exact values of n, N and statistical tests performed can be found in Table S1. All data processing and statistical analysis were performed in Excel (Microsoft) and GraphPad Prism (GraphPad Software). Significance was defined as follows: n.s., not significant; *$p < 0.05$; **$p < 0.01$; and ***$p < 0.001$. Graphs were made using GraphPad Prism.

Mass spectrometry analysis

All samples were analyzed on an Orbitrap Q-Exactive mass spectrometer (Thermo Fisher Scientific) coupled to an Agilent 1290 Infinity LC (Agilent Technologies). Peptides were loaded onto a trap column (Reprosil C18, 3 μm, 2 cm × 100 μm; Dr. Maisch) with solvent A (0.1% formic acid in water) at a maximum pressure of 800 bar and chromatographically separated over the analytical column (Zorbax SB-C18, 1.8 μm, 40 cm × 50 μm; Agilent) using 90 min linear gradient from 7%–30% solvent B (0.1% formic acid in acetonitrile) at a flow rate of 150 nL/min. The mass spectrometer was used in a data-dependent mode, which automatically switched

between MS and MS/MS. After a survey scan from 350- 1500 m/z the 10 most abundant peptides were subjected to HCD fragmentation. Raw files were processed using Proteome Discoverer 1.4 (Thermo Scientific). Database searches were performed either using the human Uniprot database or the rat Uniprot database and Mascot (version 2.5.1, Matrix Science, UK) as search engine. Carbamidomethylation of cysteines was set as a fixed modification and oxidation of methionine was set as a variable modification. Trypsin was set as cleavage specificity, allowing a maximum of 2 missed cleavages. Data filtering was performed using percolator, resulting in 1% false discovery rate (FDR). Additional filters were search engine rank 1 and mascot ion score > 20.

Image analysis and quantification

Image processing, analysis and quantifications were performed using ImageJ (Abràmoff, Magalhães and Ram, 2004) and Fiji (Schindelin et al., 2012). Recording settings were kept the same for all conditions in each experiment.

Analysis of neuronal morphology

For the analysis of axon morphology, the axon was identified based on morphology (pβactin-GFP or GW2-GFP was used as a fill, which signal was increased by immunostaining with a GFP antibody) and the presence of TRIM46 marker in one neurite. The axon was traced using ImageJ software and the NeuronJ plugin (Meijering et al., 2004). The total axon length was calculated as the sum of the longest axonal branch (primary branch) and all its side branches. Only branches longer than 8 μm were included in this analysis.

For analysis of dendritic development, the dendrites were identified based on morphology (pβactin-GFP or GW2-GFP was used as a fill, which signal was increased by immunostaining with a GFP antibody) and the absence of TRIM46 marker. Dendrites were traced using ImageJ software and the NeuronJ plugin and further analysis was performed using the Sholl Analysis plugin v3.4.5 (Meijering et al., 2004; Ferreira et al., 2014). The first circle was defined by the soma size and subsequent circles with increased 10 μm steps up to 100 μm distance from the cell body. Only branches longer than 8 μm were included in this analysis.

Analysis of polarity indices

To calculate the polarity index for CAMSAP2 and CAMSAP3, both CRISPR-KI and overexpression, the average intensity of ~40 μm along the axon (starting after the AIS) or dendrite was measured. The mean intensities of two dendrites, with a similar diameter to the axon, were averaged and background was subtracted using ImageJ. Polarity index (PI) was calculated with the formula: PI = (Id-Ia)/(Id+Ia), where Id corresponds to mean dendrite intensity, while Ia is the mean axon intensity. PI > 0 indicates the polarization is biased toward dendrite and PI < 0 to the axon.

Colocalization analysis in COS-7 cells

Transfected COS-7 cells with low expression levels of CAMSAP2 and WDR47 were used in the analysis. Gaussian Blur filter of 1 pixel was applied to images using FIJI. WDR47 and CAMSAP2 particles were detected and colocalization analysis was performed using FIJI ComDet plugin v.0.5.0 (https://github.com/ekatrukha/ComDet). Values of 'approximate pixel size' and 'intensity threshold' were chosen to detect WDR47 and CAMSAP2 particles with puncta and stretch-like appearances. CAMSAP2 detected particles were categorized into WDR47- colocalized and non-colocalized particles. Intensity and area of CAMSAP2 particles were obtained from the output table from the ComDet plugin to calculate density (intensity/area).

Microtubule severing by photoablation

Background subtraction was performed on each channel and then Gaussian Blur filter of 1 pixel was applied to images. ROI was selected around the minus end of the severed microtubule to measure the intensity of CAMSAP2 and WDR47 in each frame. Intensities were normalized to the intensity in the first frame after microtubule severing. For plotting (Figure S3C) the moving time average of 5 frames was calculated.

Quantification of CAMSAP2 staining

To quantify the amount of endogenous CAMSAP2 stretches, maximum intensity projections were made of confocal acquisitions covering the entire soma of both transfected and non-transfected (NT) neurons on each coverslip. To overcome the issue of staining variation between coverslips, we continued with the following unbiased approach: First, we determined for 5 NT neurons per coverslip an intensity threshold that would highlight their CAMSAP2 stretches (using "Threshold" function of ImageJ software). Next, their average threshold value was calculated and applied to all (both transfected and NT neurons) within that coverslip, resulting in a binary mask for each neuron of soma area covered by CAMSAP2 particles. We could then 1) use this masked selection to calculate for each neuron the ratio of masked CAMSAP2-containing area/total soma area, after which the transfected neurons were normalized to the average of NT neurons within that coverslip. Furthermore, we could 2) detect the number of distinct particles present within the masked CAMSAP2-containing area using the "Analyze particles" function of ImageJ software. We then calculated the number of particles per 10 μm^2 of soma, and normalized the number of particles / μm^2 soma of transfected neurons to the average of NT neurons within the coverslip. Particles < 0.05 μm^2 were excluded from this analysis.

Cell Reports, Volume *36*

Supplemental information

WDR47 protects neuronal microtubule minus ends from katanin-mediated severing

Robin R. Buijs, Jessica J.A. Hummel, Mithila Burute, Xingxiu Pan, Yujie Cao, Riccardo Stucchi, Maarten Altelaar, Anna Akhmanova, Lukas C. Kapitein, and Casper C. Hoogenraad

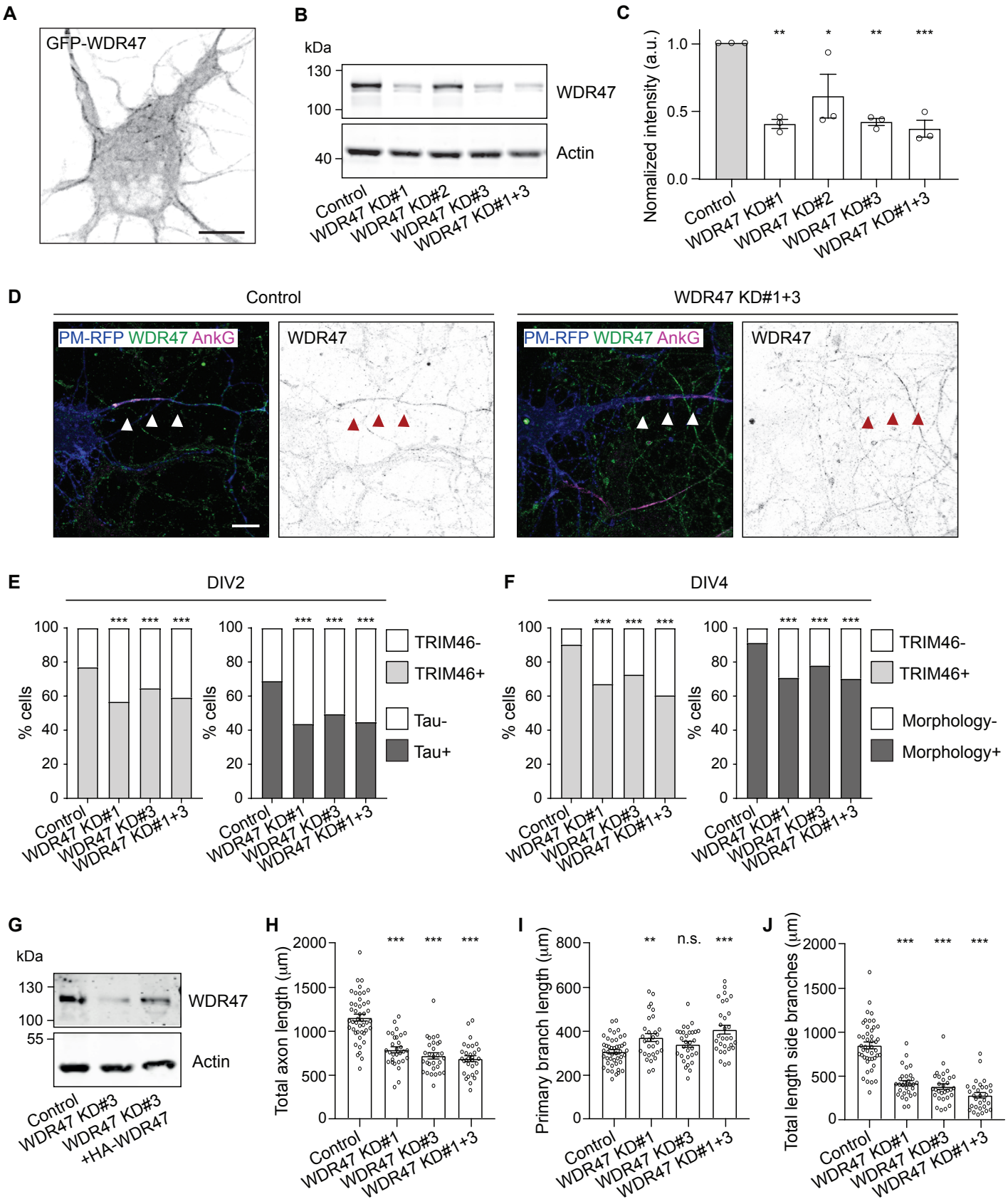
A
GFP-WDR47
B
kDa
130
100
40
WDR47
Actin
Control
WDR47 KD#1
WDR47 KD#2
WDR47 KD#3
WDR47 KD#1+3
C
Nomalized intensity (a.u.)
1.0
0.5
0.0
**
*
**
***
D
Control
WDR47 KD#1+3
PM-RFP WDR47 AnkG
WDR47
E
DIV2
% cells
100
80
60
40
20
0
***
TRIM46-
TRIM46+
Tau-
Tau+
F
DIV4
Morphology-
Morphology+
G
kDa
130
100
55
WDR47
Actin
Control
WDR47 KD#3
WDR47 KD#3
+HA-WDR47
H
Total axon length (µm)
2000
1500
1000
500
0
I
Primary branch length (µm)
800
600
400
200
n.s.
J
Total length side branches (µm)

Figure S1. Related to Figure 1. WDR47 is important for neuronal development.

(A) Spinning disk confocal microscopy image of a live DIV10 hippocampal neuron transfected with GFP-WDR47.

(B) Western blot analysis of cell lysates from DIV4 cortical neurons electroporated at DIV0 with pSuper Control, WDR47 KD#1, WDR47 KD#3 or WDR47 KD#1+3 shRNAs with indicated antibodies.

(C) Quantification of WDR47 levels related to B. Data was normalized to actin (loading control) and the pSuper control (N=3).

(D) Maximum intensity projections of DIV7 hippocampal neurons co-transfected for 96 hrs with plasma membrane marker PM-RFP (blue) as transfection marker and pSuper Control or WDR47 shRNA#1+3 (WDR47 KD#1+3), stained for WDR47 (green) and Ankyrin-G (magenta). Arrows indicate axon.

(E) Quantification of DIV2 hippocampal neurons electroporated at DIV0 with GFP and pSuper Control or WDR47 KD#1, WDR47 KD#3 or WDR47 KD#1+3 shRNAs showing the percentage of neurons with neurites positive for endogenous TRIM46 (left) or Tau (right) (N=2, n=296-338).

(F) Quantification of DIV4 hippocampal neurons electroporated at DIV0 with GFP and pSuper Control or WDR47 KD#1, WDR47 KD#3 or WDR47 KD#1+3 shRNAs showing the percentage of neurons with neurites positive for endogenous TRIM46 (left) or a polarized morphology showing one neurite at least 2x longer than other neurites (right) (N=2-3, n=300-464).

(G) Western blot analysis of cell lysates from DIV4 cortical neurons electroporated at DIV0 with pSuper Control, WDR47 KD#3 or WDR47 KD#3 + HA-WDR47 with indicated antibodies.

(H, I, J) Quantification of total axon length (H), longest axon branch (I) or total length of all side branches (J) of DIV4 hippocampal neurons electroporated at DIV0 with GFP and pSuper Control or WDR47 KD#1, WDR47 KD#3 or WDR47 KD#1+3 shRNAs (N=3, n=45 for Control, N=2, n=30 for WDR47 shRNAs).

Graphs represent mean ± SEM. *$p < 0.05$, **$p < 0.01$, ***$p < 0.001$. See Table S1. Scale bars: 10μm.

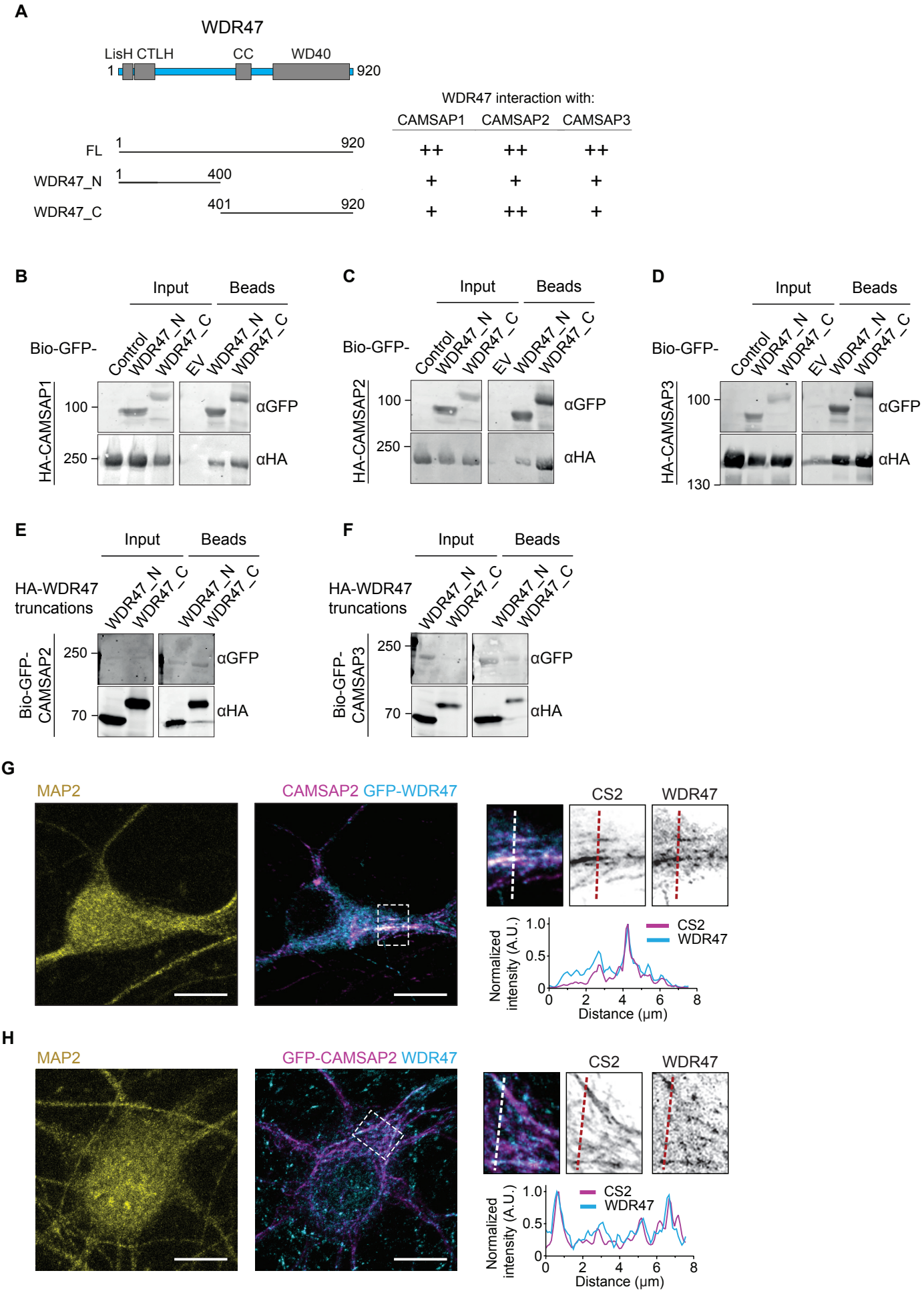
A
WDR47
LisH CTLH
CC
WD40
1
920
WDR47 interaction with:
CAMSAP1 CAMSAP2 CAMSAP3
FL 1 920 ++ ++ ++
WDR47_N 1 400 + + +
WDR47_C 401 920 + ++ +
B
Input
Beads
Bio-GFP-
Control
WDR47_N
WDR47_C
EV
HA-CAMSAP1
100
250
αGFP
αHA
C
HA-CAMSAP2
D
HA-CAMSAP3
130
E
HA-WDR47 truncations
Bio-GFP-CAMSAP2
70
F
Bio-GFP-CAMSAP3
G
MAP2
CAMSAP2 GFP-WDR47
CS2
WDR47
Normalized intensity (A.U.)
1.0
0.5
0
2
4
6
8
Distance (μm)
H
GFP-CAMSAP2 WDR47

Figure S2. Related to Figure 2. WDR47 interacts with CAMSAP family proteins.

(A) Schematic depiction of the domain structure of WDR47 and the constructs/ truncations used for pulldowns shown in this figure. Indicated domains: CC, coiled coil; CTLH, C-terminal to LisH domain; LisH, lissencephaly-1 homology domain; WD40, WD40 repeat domain.

(B, C, D) Western blot analysis of streptavidin pulldown assay using extracts of HEK293T cells transfected with BirA and HA-CAMSAP1 (B), HA-CAMSAP2 (C) or HA-CAMSAP3 (D) constructs (bait) and Bio-GFP (Control), Bio-GFP-WDR47_C or Bio-GFP-WDR47_N (prey), with indicated antibodies.

(E, F) Western blot analysis of streptavidin pulldown assay using extracts of HEK293T cells transfected with BirA and Bio-GFP- CAMSAP2 (E) or Bio-GFP-CAMSAP3 (F) constructs (prey) and HA-WDR47_N and HA-WDR47_C (bait), with indicated antibodies.

(G and H) Representative images of DIV11 hippocampal neurons transfected with GFP-WDR47 and co-stained for endogenous CAMSAP2 (G) or transfected with GFP-CAMSAP2 and co-stained for endogenous WDR47 (H), combined with GFP antibody (to enhance the signal in transfected cells) and MAP2 (yellow) staining. Zooms are indicated by dashed boxes and show somatodendritic regions. Intensity profiles show the normalized intensity of both channels along the dashed line indicated in the zooms.

Scale bars: 10μm.

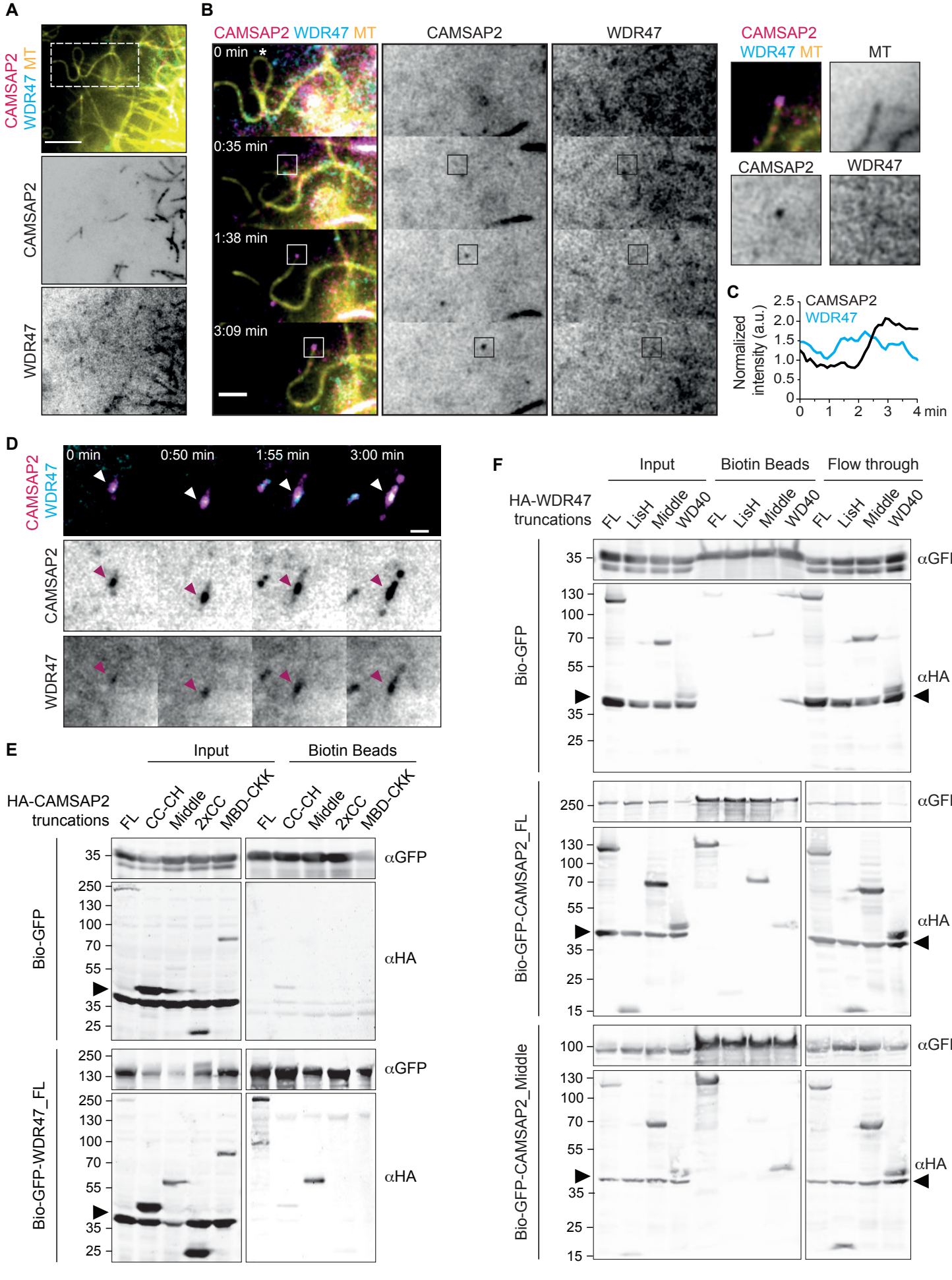
A
CAMSAP2 WDR47 MT
CAMSAP2
WDR47
B
CAMSAP2 WDR47 MT
CAMSAP2
WDR47
0 min
0:35 min
1:38 min
3:09 min
CAMSAP2 WDR47 MT
MT
CAMSAP2
WDR47
C
Normalized intensity (a.u.)
CAMSAP2
WDR47
4 min
D
CAMSAP2 WDR47
0 min
0:50 min
1:55 min
3:00 min
CAMSAP2
WDR47
E
Input
Biotin Beads
HA-CAMSAP2 truncations
FL
CC-CH
Middle
2xCC
MBD-CKK
Bio-GFP
Bio-GFP-WDR47_FL
αGFP
αHA
F
Input
Biotin Beads
Flow through
HA-WDR47 truncations
FL
LisH
Middle
WD40
Bio-GFP
Bio-GFP-CAMSAP2_FL
Bio-GFP-CAMSAP2_Middle
αGFP
αHA

Figure S3. Related to Figure 3. WDR47 localizes to MT minus ends along with CAMSAP2.

(A) TIRF image of a COS-7 cell with MTs stained using SiR-tubulin (yellow), transfected with 3GFP-CAMSAP2 (magenta) and mCherry-WDR47 (cyan). Zoom is indicated by dashed box.

(B) Zoom related to A. A single MT (indicated by white box) was severed by photoablation to generate new minus end. * indicates place of laser severing. Boxes are drawn around MT minus end to visualize CAMSAP2 and WDR47 localization. Zoom panels show boxes of all channels at last time point (3:09 min). See also Video S1.

(C) Quantification of CAMSAP2 and WDR47 intensity at new MT minus end relative to the first time frame after MT-severing. Moving time average of 5 frames was used for the plot.

(D) Example of small CAMSAP2 (magenta) puncta growing into a long stretch. WDR47 (cyan) colocalizes strongly as the CAMSAP2 puncta grows. See also Video S2.

(E) Western blot analysis of streptavidin pulldown assay using extracts of HEK293T cells transfected with BirA and indicated HA-CAMSAP2 truncations (bait) and Bio-GFP-WDR47_FL or Bio-GFP (prey) as a negative control with indicated antibodies. Arrow head indicate triple HA-tag of BirA construct.

(F) Western blot analysis of streptavidin pulldown assay using extracts of HEK293T cells transfected with BirA and indicated HA-WDR47 truncations (bait) and Bio-GFP-CAMSAP2_FL, Bio-GFP-CAMSAP2_Middle or Bio-GFP (prey) as a negative control with indicated antibodies. Arrow heads indicate triple HA-tag of BirA construct.

Scale bars: 5μm in (A) and 2μm in (B).

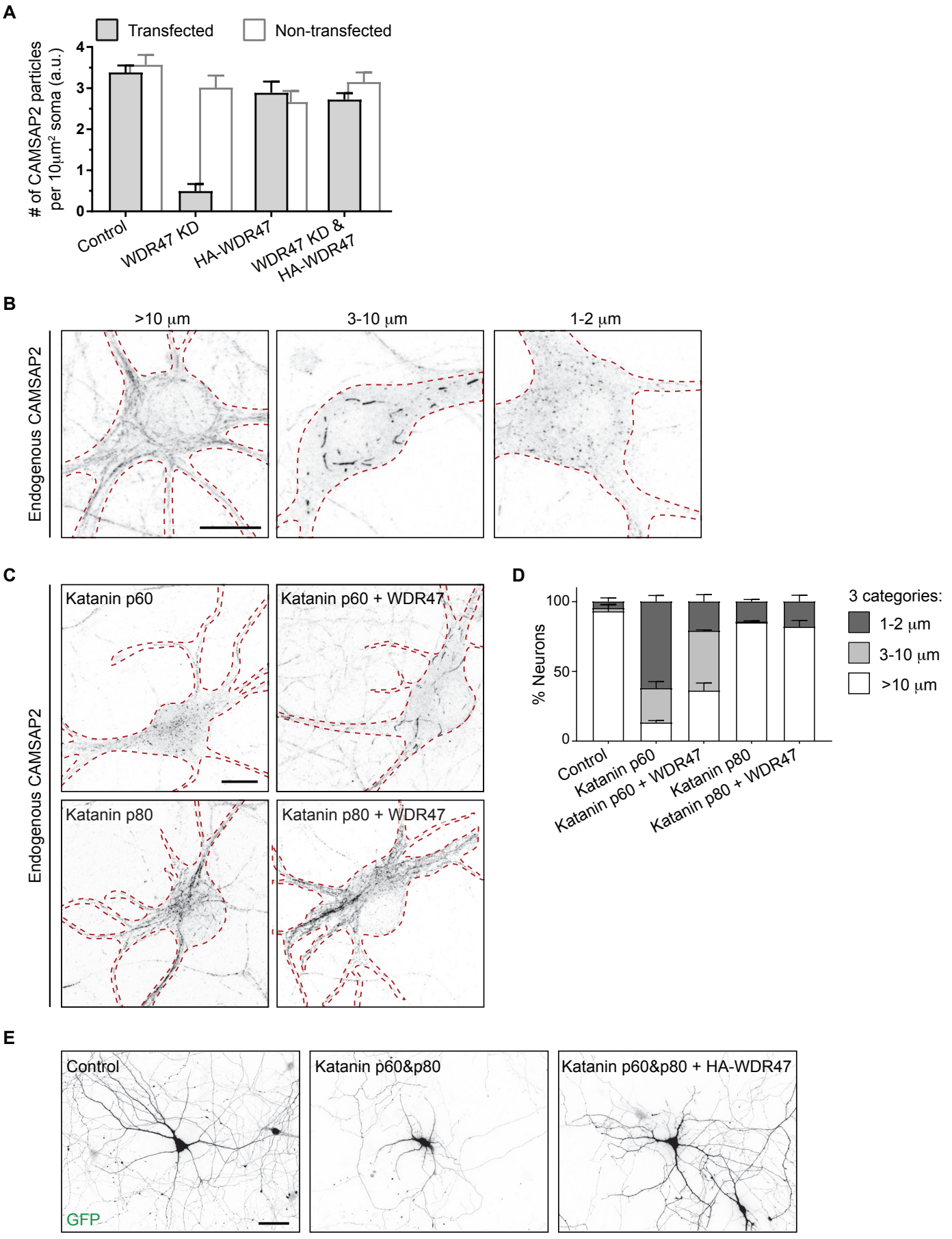
A
Transfected
Non-transfected
# of CAMSAP2 particles per 10μm² soma (a.u.)
0
1
2
3
4
Control
WDR47 KD
HA-WDR47
WDR47 KD & HA-WDR47
B
>10 μm
3-10 μm
1-2 μm
Endogenous CAMSAP2
C
Katanin p60
Katanin p60 + WDR47
Katanin p80
Katanin p80 + WDR47
Endogenous CAMSAP2
D
% Neurons
0
50
100
Control
Katanin p60
Katanin p60 + WDR47
Katanin p80
Katanin p80 + WDR47
3 categories:
1-2 μm
3-10 μm
>10 μm
E
Control
GFP
Katanin p60&p80
Katanin p60&p80 + HA-WDR47

Figure S4. Related to Figure 4. WDR47 protects CAMSAP2 stretches from Katanin.

(A) Average absolute number of CAMSAP2 puncta detected per 10μm^2 soma related to Figure 4C. Values of non-transfected neurons within the same coverslip are shown behind each condition (N=3, n=21-22 and n=15 for NT neurons).

(B) Representative example images of CAMSAP2 staining patterns that are categorized as: long (>10μm), medium (3-10μm) or short (1-2μm) stretches. Cell outlines are indicated with red dashed lines.

(C) Maximum intensity projections of CAMSAP2 immunostaining in DIV10 hippocampal neurons co-transfected for 48 hrs with transfection marker BFP and mCherry-KataninP60, mCherry-KataninP80, or mCherry-KataninP60/P80 plus HA-WDR47. Cell outlines are indicated with red dashed lines.

(D) Quantification of CAMSAP2 staining pattern per condition related to C categorized according to B (N=2-3, n=96-193).

(E) Widefield images of DIV10 hippocampal neurons co-transfected for 48 hrs with GFP and mCherry, mCherry-KataninP60+p80, or mCherry-KataninP60+p80 and HA-WDR47. Related to Figure 4 F-G.

Graphs represent mean ± SEM. See Table S1. Scale bars: 10μm in (B) and (C) and 50μm in (E).

Table S1. Overview of the data and statistical analysis in this study. Related to Figure 1-4 and Figure S1 and S4.

Figure	Sample sizes (N & n)	Statistical test	Values
1B	N=2 batches, n=4 blots	-	(2 biological replicates and 2 technical replicates of each)
1E	N=2 experiments, n= 20 neurons per condition	One Way ANOVA with Dunnett's multiple comparisons test	One Way ANOVA F (DFn, DFd) = F (3, 76) = 9.47, p<0.0001 Dunnett's multiple comparisons test Control x WDR47 KD: p<0.0001 Control x HA-WDR47: p=0.6425 Control x WDR47 KD + HA-WDR47: p=0.1286
1F	N=2 experiments, n= 20 neurons per condition	One Way ANOVA with Dunnett's multiple comparisons test	One Way ANOVA F (DFn, DFd) = F (3, 76) = 2.823, p=0.0444 Dunnett's multiple comparisons test Control x WDR47 KD: p=0.0615 Control x HA-WDR47: p=0.6305 Control x WDR47 KD + HA-WDR47: p=0.9749
1G	N=2 experiments, n= 20 neurons per condition	One Way ANOVA with Dunnett's multiple comparisons test	One Way ANOVA F (DFn, DFd) = F (3, 76) = 12.17, p<0.0001 Dunnett's multiple comparisons test Control x WDR47 KD: p<0.0001 Control x HA-WDR47: p=0.4624 Control x WDR47 KD + HA-WDR47: p=0.1628
1I	N=2 experiments, n= 20 neurons per condition	-	
1J	N=2 experiments, n= 20 neurons per condition	One Way ANOVA with Dunnett's multiple comparisons test	One Way ANOVA F (DFn, DFd) = F (3, 76) = 10.17, p<0.0001 Dunnett's multiple comparisons test Control x WDR47 KD: p<0.0001 Control x HA-WDR47: p=0.4177 Control x WDR47 KD + HA-WDR47: p=0.2808
2D	GFP-CS2 KI: N=2, n=7 GFP-CS3 KI: N=2, n=15		
2E	GFP-CS2 OE: N=2, n=12 GFP-CS3 OE: N=2, n=8		
3C	N=7 cells Colocalized: n= 144 Non-colocalized: n= 129	Mann Whitney U test	Colocalized x Non-colocalized: U=2912, p<0.0001
3D	N=7 cells Colocalized: n= 145 Non-colocalized: n= 129	Mann Whitney U test	Colocalized x Non-colocalized: U=4731, p<0.0001
3E	N=7 cells Colocalized: n= 145 Non-colocalized: n= 130	Mann Whitney U test	Colocalized x Non-colocalized: U=2898, p<0.0001
4B	Control: N=3, n=22 WDR47 KD: N=3, n=21 HA-WDR47: N=3, n=21 WDR47 KD+HA-WDR47: N=3, n=21	Kruskal-Wallis test with Dunn's multiple comparisons test	Kruskal-Wallis test H (χ2) = 46.84; p<0.0001 Dunn's multiple comparisons test Control x WDR47 KD: p<0.0001 Control x HA-WDR47: p>0.9999 Control x WDR47 KD+HA-WDR47: p>0.9999
4C	Control: N=3, n=22 WDR47 KD: N=3, n=21 HA-WDR47: N=3, n=21 WDR47 KD+HA-WDR47: N=3, n=21	Kruskal-Wallis test with Dunn's multiple comparisons test	Kruskal-Wallis test H (χ2) = 42.09; p<0.0001 Dunn's multiple comparisons test Control x WDR47 KD: p<0.0001 Control x HA-WDR47: p>0.9999 Control x WDR47 KD+HA-WDR47: p>0.9999
4E	Control: N-2, n=91 Katanin p60&p80: N=3, n=171 Katanin p60&p80 + WDR47: N=3, n=178		
4F	N=2 experiments, n= 20 neurons per condition		

4G	N=2 experiments, n= 20 neurons per condition	One Way ANOVA with Dunnett's multiple comparisons test	One Way ANOVA F (DFn, DFd) = F (2, 57) = 13.81, p<0.0001 Dunnett's multiple comparisons test Control x Katanin p60&p80: p<0.0001 Control x Katanin p60&p80 + HA-WDR47: p=0.2754
S1C	3 individual experiments	One Way ANOVA with Dunnett's multiple comparisons test	One Way ANOVA F (DFn, DFd) = F (4,10) = 11.03 p=0.0011 Dunnett's multiple comparisons test Control x WDR47 KD#1: p=0.0012 Control x WDR47 KD#2: p=0.0186 Control x WDR47 KD#3: p=0.0014 Control x WDR47 KD#1+3: p=0.0008
S1E	Control: N=2, n=296 cells WDR47 KD#1: N=2, n=338 cells WDR47 KD#3: N=2, n=329 cells WDR47 KD#1+3: N=2, n=321 cells	Two-tailed Fisher's exact test	TRIM46 Control x WDR47 KD#1: p<0.0001 Control x WDR47 KD#3: p=0.0008 Control x WDR47 KD#1+3: p<0.0001 Tau Control x WDR47 KD#1: p<0.0001 Control x WDR47 KD#3: p<0.0001 Control x WDR47 KD#1+3: p<0.0001
S1F	Control: N=3, n=404 cells WDR47 KD#1: N=2, n=302 cells WDR47 KD#3: N=2, n=300 cells WDR47 KD#1+3: N=2, n=464 cells	Two-tailed Fisher's exact test	TRIM46 Control x WDR47 KD#1: p<0.0001 Control x WDR47 KD#3: p<0.0001 Control x WDR47 KD#1+3: p<0.0001 Morphology Control x WDR47 KD#1: p<0.0001 Control x WDR47 KD#3: p<0.0001 Control x WDR47 KD#1+3: p<0.0001
S1H	Control: N=3, n=45 KDs: N=2, n=30	One Way ANOVA with Dunnett's multiple comparisons test	One Way ANOVA F (DFn, DFd) = F (3, 131) = 39.20, p<0.0001 Dunnett's multiple comparisons test Control x WDR47 KD#1: p<0.0001 Control x WDR47 KD#3: p<0.0001 Control x WDR47 KD#1+3: p<0.0001
S1I	Control: N=3, n=45 KDs: N=2, n=30	One Way ANOVA with Dunnett's multiple comparisons test	One Way ANOVA F (DFn, DFd) = F (3, 131) = 8.882, p<0.0001 Dunnett's multiple comparisons test Control x WDR47 KD#1: p=0.0053 Control x WDR47 KD#3: p=0.2374 Control x WDR47 KD#1+3: p<0.0001
S1J	Control: N=3, n=45 KDs: N=2, n=30	One Way ANOVA with Dunnett's multiple comparisons test	One Way ANOVA F (DFn, DFd) = F (3, 131) = 58.89, p<0.0001 Dunnett's multiple comparisons test Control x WDR47 KD#1: p<0.0001 Control x WDR47 KD#3: p<0.0001 Control x WDR47 KD#1+3: p<0.0001
S4A	Related to Figure 4C		
S4D	Control: N-2, n=161 Katanin p60: N=3, n=166 Katanin p60 + WDR47: N=3, n=193 Katanin p80: N=3, n=165 Katanin p80 + WDR47: N=2, n=96		